Transnational conservation to anticipate future plant shifts in Europe

Preprint · March 2023

DOI: 10.21203/rs.3.rs-2599463/v1

8 authors, including:

Yohann Chauvier-Mendes
Swiss Federal Institute for Forest, Snow and Landscape Research WSL
11 PUBLICATIONS **203** CITATIONS
SEE PROFILE

Peter H Verburg
Vrije Universiteit Amsterdam
669 PUBLICATIONS **48,386** CITATIONS
SEE PROFILE

Dirk Nikolaus Karger
Swiss Federal Institute for Forest, Snow and Landscape Research WSL
147 PUBLICATIONS **6,291** CITATIONS
SEE PROFILE

Loïc Pellissier
ETH Zurich/ WSL Birmensdorf
276 PUBLICATIONS **11,638** CITATIONS
SEE PROFILE

Transnational conservation to anticipate future plant shifts in Europe

Yohann Chauvier Mendes (yohann.chauvier@wsl.ch)
Swiss Federal Institute for Forest, Snow and Landscape Research https://orcid.org/0000-0001-9399-3192

Laura Pollock
McGill

Peter H. Verburg
Vrije Universiteit Amsterdam

Dirk Nikolaus Karger
Swiss Federal Research Institute WSL https://orcid.org/0000-0001-7770-6229

Loïc Pellissier
ETH Zürich https://orcid.org/0000-0002-2289-8259

Sébastien Lavergne
CNRS

Niklaus Zimmermann
Swiss Federal Research Institute WSL https://orcid.org/0000-0003-3099-9604

Wilfried Thuiller
Univ. Grenoble Alpes - CNRS

Biological Sciences - Article

Keywords:

Posted Date: March 30th, 2023

DOI: https://doi.org/10.21203/rs.3.rs-2599463/v1

Additional Declarations: There is **NO** Competing Interest.

Title: Transnational conservation to anticipate future plant shifts in Europe

Authors: Yohann Chauvier[1]*, Laura J. Pollock [2], Peter H. Verburg [1,3], Dirk N. Karger [1], Loïc Pellissier[1,4], Sébastien Lavergne[5], Niklaus E. Zimmermann[1], Wilfried Thuiller[5]

[1]Swiss Federal Research Institute (WSL); 8903 Birmensdorf, Switzerland

[2]Department of Biology, McGill University; Montreal, QC H3A 1B1, Canada.

[3]Environmental Geography Group, Institute for Environmental Studies, Vrije Universiteit; Amsterdam, De Boelelaan 1085, 1081HV Amsterdam, Netherlands.

[4]Landscape Ecology, Institute of Terrestrial Ecosystems, Department of Environmental Systems Science, Eidgenössische Technische Hochschule (ETH) Zürich; 8092 Zürich, Switzerland.

[5]Univ. Grenoble Alpes, Univ. Savoie Mont Blanc, CNRS, LECA, Laboratoire d'Ecologie Alpine ; F-38000 Grenoble, France.

*Corresponding author. Email: yohann.chauvier@wsl.ch

Abstract: To meet the COP15 biodiversity framework in Europe, one target is to protect 30% of land by 2030 through a resilient transnational conservation network [1,2]. The European Alps are a key hub of this network hosting one of the most extensive natural areas and hotspots of plant biodiversity in Europe [3,4]. Here, we assess the robustness of the conservation network to safeguard the European Alps' flora by 2080 using semi-mechanistic simulations. Overall, we predict a shift in conservation need from lower to higher elevations through time as plants migrate upslope and shrink their distribution. While increasing species, trait, and evolutionary diversity, migration could also threaten 70% of the resident flora. Future expansions of the protected area network should ensure strong elevational connections, even those that span borders.

Main Text:

In line with the recent COP15 biodiversity framework of the Convention on Biological Diversity (CBD), the European Union (EU) seeks to implement a coherent and resilient transnational nature protection network by 2030 covering at least 30% of the EU's land. The *EU Biodiversity Strategy for 2030* [1,2] specifies the necessity to improve the European protected area network by further implementing transboundary protected areas to effectively preserve biological biodiversity and nature contributions to people under global change in the future. Central to this conservation network, the European Alps are one of the largest semi-natural areas of the continent and a centre of plant diversity and endemism [3,4]. Spread across seven countries, the Alps host ~4,500 vascular plant species – more than the third of the flora recorded in Western Europe – with around 400 endemic species [3], and unveils a long history of land use and geographical processes that has shaped evolutionary and phenotypic plant adaptations over time [5,6].

Alpine and mountain ecosystems are altered by global change in a complex way [7–12]. Many species are expected to migrate upwards increasing the risk of extinction for cold-adapted alpine plants that have limited colonization opportunity and potentially suffering from competitive exclusion [13–15]. In the European Alps, not only climate, but also land use change, is expected to affect this species redistribution, as agricultural land abandonment at high elevation and human activities such as intensification in the lowlands negatively impact mountain biodiversity in Europe [5,16]. While protected areas (PAs) are static entities aimed at preserving biological biodiversity, their networks in mountain ecosystems are generally known to be biased towards higher elevations [17,18], with endangered species sometimes anticipated to naturally migrate within these networks [19]. Therefore, the effectiveness of PAs is also dependent on climate change and changes in land use affecting natural areas, inside and outside these PAs. In this context, we must quantify how species are likely to migrate under global change [20], which species will become threatened, and how the current conservation network should be transnationally adapted to future species range shifts and local extinctions.

Climate and land-use change are expected to influence different facets of biodiversity in different ways, requiring a multi-dimensional approach to conservation [19,21]. Biodiversity is not only about individual species, but is rather about 'diversity'— how many species are found in an area or conservation unit (species richness), how much evolutionary history is shared among those species (phylogenetic diversity) [22], and how diverse are their morphological traits and roles (functional diversity) [23]. From a conservation planning perspective, it is useful to also consider how each local area contributes to the unique biodiversity of the region (e.g. species or functions not found elsewhere), that can be measured as species- [24], phylogenetic- [25], or functional endemism [26]. Finally, 'rarity', which estimates scarcity of unique traits [27] or phylogenetic branches [28], also contributes to 'diversity' and deserve to be considered. It is therefore crucial that conservation planning embraces all these facets to optimize protection complementarity and irreplaceability between geographic areas.

Here, we investigate the efficiency of the current European Alps' PAs network, and of its potential transnational expansion, in protecting the plant multifaceted diversity and uniqueness of this region at present and for the 2050 and 2080 horizons, under biologically informed (realistic) dispersal, two Shared Socioeconomic Pathways (SSPs), seven Global

Circulation Model (GCMs) and two land cover (LC) change scenarios. Using an ensemble of species distribution models (SDMs) for 1,711 plant species at 100-m resolution, a high coverage database of species traits and two mega-phylogenies, we predicted future changes in species distributional range, multifaceted diversity and uniqueness in the study area. We then identified conservation priorities for all types of diversity, areas where these priorities are stable into the future (overlap in current and future priorities), and areas that are critical for expanding the current PA network to meet the 2030 targets while achieving a resilient and effective conservation network.

Upward shifts of multifaceted diversity

Overall, our SDM approach demonstrates very good performance with an average True Skill Statistics and Boyce Index of the kept models ranging between ~0.6 and ~0.8 across the 1,711 species considered. We show that the European Alps are predicted to lose between ~7 and 16% of its total multifaceted diversity and uniqueness by 2080 (Fig. S1a-b). This loss is expected to occur primarily at low elevations (without accounting for colonization from other regions), with corresponding gains at higher elevations due to upward species range shifts, even by 2050 and under the moderate SSP245 scenario (Fig. 1). Changes are even more exacerbated for 2080, the worst case SSP585 scenario, and under unrealistic unlimited dispersal (Fig. S2a-e). Our results are in line with previous research showing that most species are able to respond to climate change by migrating towards cooler temperatures [29–31], therefore increasing the short-term species richness of higher mountain strata [14,32,33]. On the one hand, by extending these results to species traits and evolution, we show that upslope migrations not only infer a change in species richness but also in other biodiversity facets. On the other hand, these migrations also generally result in a decrease in species range size due to limited physical habitat area, consequently explaining the positive changes in multifaceted endemism and rarity that we uncovered at higher elevation [20,34]. Additionally, we forecast that rural landscapes (e.g., permanent crops and pasture), which were found to harbour more plant diversity than forests and grasslands (Fig. S3), will suffer from future land abandonments with forest successions across large landscapes (Fig. S4). This corroborates previous studies uncovering the negative impact of land abandonment on biodiversity in the northern hemisphere [16], and further explains the future high loss of multifaceted plant diversity in the European Alps.

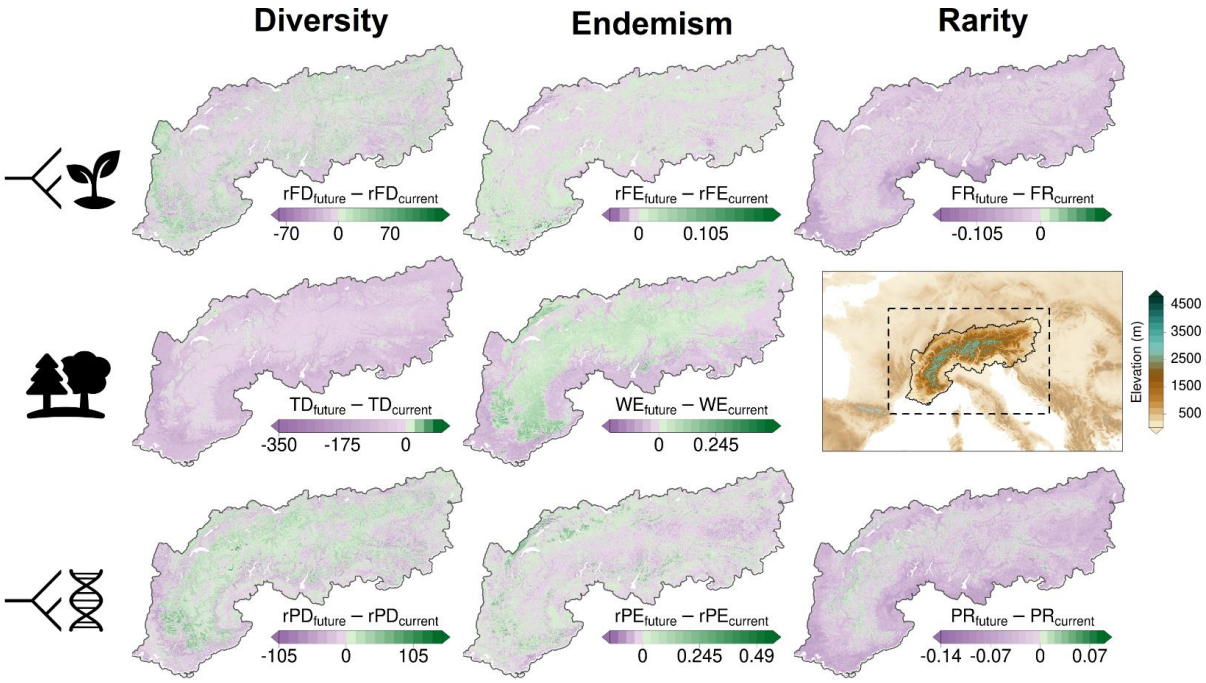

Figure 1. | Change in multifaceted diversity and uniqueness by 2050 for SSP245 and realistic plant dispersal. First, second and third row depict the functional, taxonomic and phylogenetic dimension respectively. Spatial gains are shown in green, spatial losses are shown in purple. TD, rPD and rFD: taxonomic, relative phylogenetic and relative functional diversity (relative diversity represents the diversity expected under a given taxonomic diversity, see methods); WE, rPE and rFE: weighted taxonomic, relative phylogenetic and functional endemism respectively; PR and FR: phylogenetic and functional rarity.

Species turnover and extinctions

Overall, ~70% of species are predicted to lose areas of suitable conditions ('losers'), especially in higher mountain strata (Fig. 2), and to a greater extent by 2080 under SSP585 (Fig. S5a-c). The percentage of species losing the most their suitable habitat increases from 2.1% by 2050 under SSP245 (Fig. 2) to 16.1% by 2080 for SSP585 (Fig. S5c). Many lowland species are instead forecast to experience strong range expansion ('winners', Fig. 2) with larger gains by 2080 for SSP585 (Fig. S5a-c). The percentage of species expanding the most their suitable habitat increases from 0.6% by 2050 for SSP245 (Fig. 2) to 4.2% by 2080 under the worst case SSP585 scenario (Fig. S5c). On the one hand, the range losses illustrate how loser species that are generally more restricted to specific environmental conditions are forced to migrate upwards, losing physical habitat area, facing more physical barriers to dispersal, and therefore suffering from local population extinction ('dispersal lags') [15,20,35]. On the other hand, the range expansions illustrate winner species that are abler to adapt to novel environmental conditions (e.g. thermophilic generalist species), inhabiting the lowlands, therefore conserving more range and expanding their distribution towards higher latitudes and elevations in the future [14,15,36,37]. This progressive species replacement across elevations is generally expected to increase over time and with increased global change [14,15]. Our results suggest that by the end of the 21st century, this climate-induced turnover will intensify, likely homogenizing the European Alps' plant communities (Fig. S5a-c) and possibly driving two plant species to extinction (*Antirrhinum latifolium* and *Iberis saxatilis*, Table S1). However, since we did not

account for competition between plant species in this study, we lack inclusion of important drivers of population dynamics, and perhaps underestimate potential extinction [38].

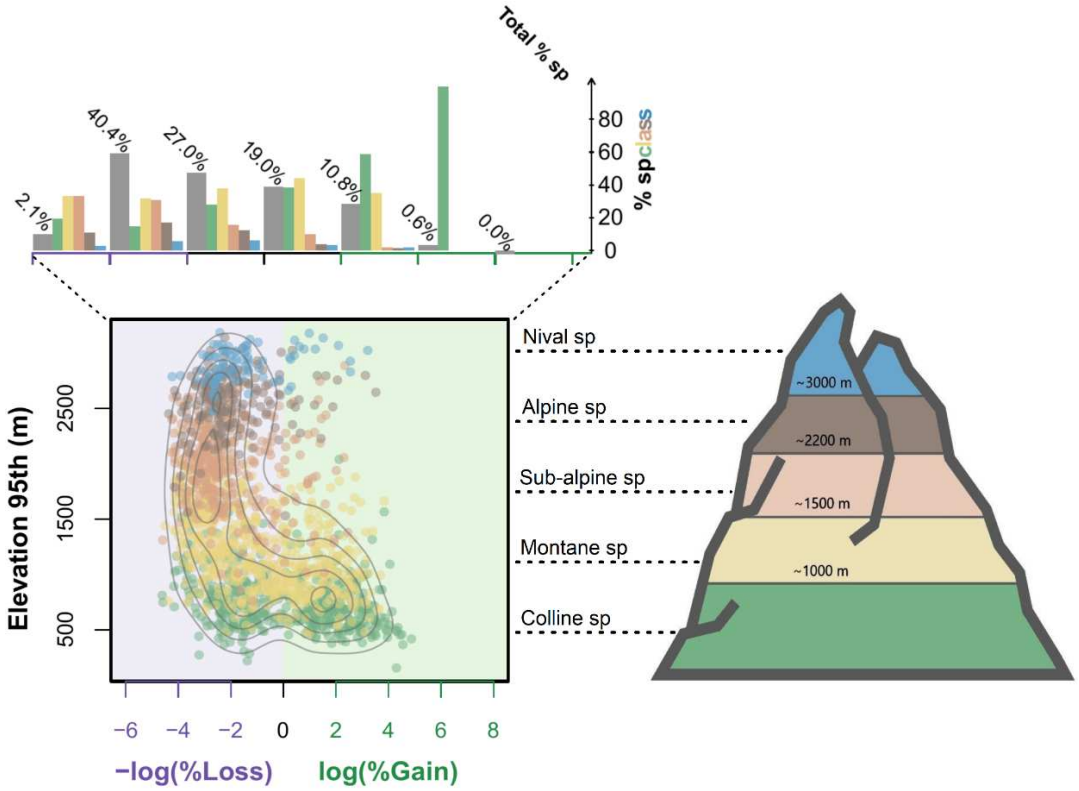

Figure 2. | Species range shifts by 2050 for SSP245 and realistic plant dispersal. The scatter plot depicts for each species (points) its 95th percentile of extracted elevation values in function of its future range gain or loss (light green and purple background respectively). Flora Alpina (FA) elevation classes were additionally assigned to each species (nival: blue, alpine: brown, sub-alpine: red, montane: yellow, colline: green) and point density contour lines were drawn for further clarity. Upper barplots summarize for each gain/loss interval the total proportion of species present (%, grey bar plots) and the relative distribution of each elevation class within.

Transnational conservation strategy

In the face of important regional changes in climate and land use, comprehensive conservation planning must be implemented with a transnational conservation strategy that mutually emphasizes local and regional conservation optimizations. On the one hand, local conservation optimization in the Alps might need little European coordination as it should focus on maximizing the local biodiversity of the region; i.e. local hotspots. On the other hand, regional conservation optimization (maximizing the biodiversity of the entire Alps) requires more transnational strategies that are implemented less often due to insufficient conservation coordination in Europe [39]. Transnational strategies should thus be improved towards coordinating complementary local and regional protective actions across distinct localities and nations, which comprise very different sets of species communities, evolutionary histories, and ecological functions [26].

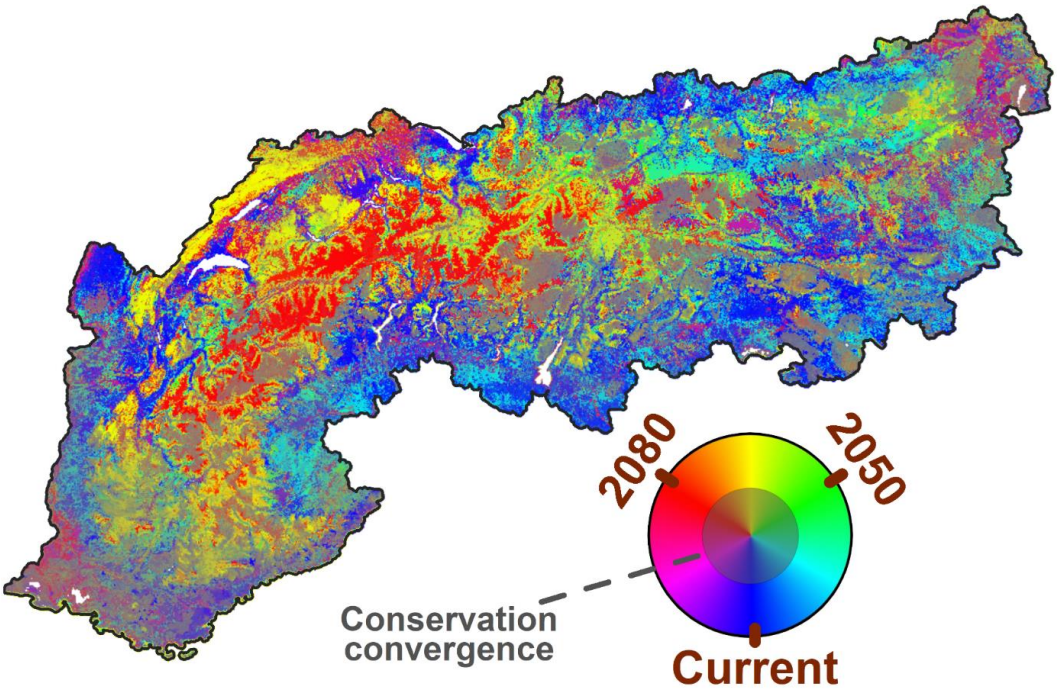

Figure 3. | Current and future local conservation needs in the European Alps for SSP245 and realistic plant dispersal. Pure colours of blue, green and red stand for largest conservation needs identified across pixels for present, 2050, and 2080, respectively. Local needs were constructed based on the current, 2050 and 2080 simulations of reserve network expansion employing the ABF prioritization algorithm (maximizing local diversity), stretched by scaling each of the three RGB colour layers and mapped as a RGB composite. Mixed colours express equally important conservation needs for two times, whereas grey stands for needs in all three times (current IUCN I-II and Natura 2000 PAs network included).

Local conservation

For local conservation strategies, we find that future conservation needs to clearly follow the expected upward shifts of plant multifaceted diversity and uniqueness under the moderate SSP245 (Fig. 3) and pessimistic SSP585 scenario (Fig. S6). Based on these results, a first clear common EU conservation strategy for the European Alps involves accommodating future plant upward migrations by increasing protected area connectivity between elevation strata. In addition to the needs for adaptive conservation in the central Alps, we also found areas of relative stability (overlapping priorities for expansion in the present and future) in the Mediterranean Alps (Fig. 3). The Mediterranean region is an endemic hotspot in Europe and is composed of distinct range-restricted and unique species [40,41]. Despite forecasted biodiversity loss, this region is still predicted to harbour high levels of multifaceted diversity and uniqueness in the future (Fig. S7-10) that are still essential to protect. Overall, similar results were also found when considering conservation needs under simulations that did not initially include current PAs (Fig. S11a-b). This emphasizes that the current PA network is insufficient to conserve biodiversity and requires adaptations to operate optimally under novel environmental conditions.

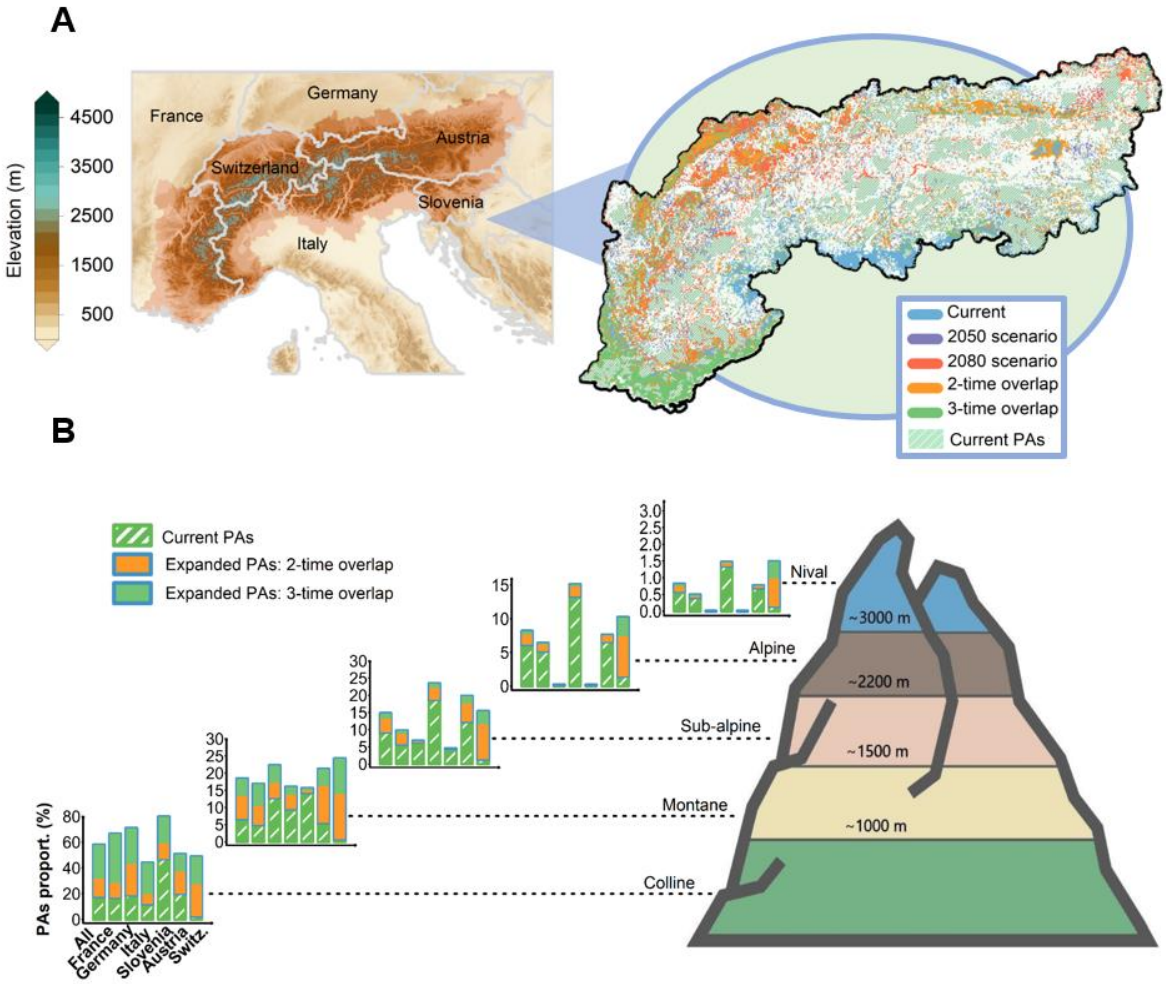

Figure 4. | Distribution of the current protected areas (PAs) network of the European Alps and its future (top 20%) regional expansion for SSP245 and realistic plant dispersal. (**A**) Left panel depicts the geographic distribution of the Alps over France, Switzerland, Germany, Austria, Slovenia and Italy, and the right panel anticipates the conservation overlaps when expanding the reserve network for present, 2050 and 2080 (top 20%). Top predicted expansions were constructed based on the current, 2050 and 2080 simulations of reserve network expansion employing the CAZ prioritization algorithm (maximizing regional diversity). (**B**) projects the conservation convergence found in (a) but distributed across each national entity (% area) and elevation strata. The current network covers ~20% of the study region and is displayed in striped green. Orange defines top expansion convergences for two timelines, whereas green is for all timelines.

Regional conservation

For regional conservation strategies, spatial future conservation needs were found to be similar although more distinct (Fig. S11c-d). While this corroborates the urgency to improve connectivity of PA across elevations in the European Alps, this also stresses the urgency for better transnational conservation in the region. In line with the COP15 diversity framework, we chose the top 20% of regional conservation expansions for current, 2050 and 2080 to project conservation overlaps, that would expand the present PAs network to ~30% of the European Alps' area, under SSP245 (Fig. 4) and SSP585 scenarios (Fig. S12). PAs are often biased towards higher elevation [18] and are generally known to be well-adapted to species upward migration induced by global change [19]. On the one hand, we confirm this tendency as

the current reserve network of the European Alps is predicted to better protect the species distribution of higher elevation strata for future timelines and SSP scenarios (Fig. S13-16). On the other hand, we detected for both SSP scenarios strong spatial (Fig. 4a) and political (Fig. 4b) divergence in optimized PA expansion, which calls for a more coherent and coordinated transnational PA network across the European Alps. As a result, the ideal contribution by France, Germany, Italy, Slovenia, Austria, and Switzerland to such an optimized strategy differ strongly among elevation belts. To balance optimal transnational contributions, Switzerland would be expected to bear the largest efforts in expanding the network across all elevation strata due to its very low PA coverage (~2% of the network, Fig. S17). Austria would be expected to increase its PAs mostly at mid-elevation. France and Germany would be expected to redirect a higher focus on lowlands, where France could best contribute to a transnational strategy by focusing on PAs in the Mediterranean Alps (Fig. 4a). This latter statement is also valid for Italy and Slovenia who would best contribute to a complementary PA network optimization by solely focusing on low to mid elevations.

Northward shifts of multifaceted diversity

Lowland Mediterranean species were also detected to strongly expand their distributional range towards higher latitudes (Fig. S18), which stresses the necessity of increasing reserve connectivity between the Mediterranean Alps and the central Alps. Species migration towards higher latitudes under global change is well documented and is expected to increase with climate change [13,30,31]. Consequently, by the end of the 21st century, the Mediterranean flora is expected to confront increasing northern barriers to dispersal, by perishing, shifting, or expanding their range upslope, dependent on their abilities to migrate, adapt to varied environmental conditions, or compete with other species. This northward migration will face a bottleneck as only few corridors exist for northward expansion, which could result in a similar depauperation of the Mediterranean flora as did Quaternary climate oscillation to the Tertiary flora [42]. Carefully conserving areas adjacent to the Mediterranean region such as the European Alps or the Pyrenees are therefore the most promising, if not the only, way to conservation of this species rich environment.

Methods:

Study area and observations

Study area

The study area covered the European Alps, as defined by an enlarged version of the official Alpine Convention perimeter [43]. The enlargement consisted of adding Switzerland entirely, as well as two French departments i.e. Ain and Bouches-du-Rhône for which we had well-documented species observations. Additionally, we extracted the International Union for Conservation of Nature (IUCN) category I-II and Natura 2000 protected areas (PAs) of the study area from the World Database on Protected Areas (WDPA; http://protectedplanet.net/).

Observations

The observational dataset used in this study was compiled from more than 77 individual sources, with largest contributions from the National Data and Information Centre on the Swiss Flora (InfoFlora; ~52%), and the Global Biodiversity Information Facility (GBIF, http://www.gbif.org/; ~29%) (see Table S2 for more information). All datasets were merged after unifying the species taxonomy, and after severely filtering inaccurate GBIF geo-referenced observations.

More specifically, to extract GBIF information and merge all datasets, a large list of synonyms of all the plant species occurring in the European Alps was generated by compiling and web-scraping information from different sources: The Catalogue of Life (http://www.catalogueoflife.org/), the Plant List (http://www.theplantlist.org/) and the French National Alpine Botanical Conservatory (CBNA). To generate this list, a search was undertaken across 4490 accepted names referenced in the Flora Alpina Atlas [44] to obtain a total of 131.660 synonyms that were used as search inputs in GBIF to retrieve our online observations using the *gbif.range* R package [45]. Only observations with a 100% confidence name matching and accurate to 11.1 meters were kept. GBIF provides a huge amount of georeferenced species distribution data, but many observations have considerable coordinate uncertainties, duplicated records, or misleading raster centroids. Therefore, strong spatial and resolution filtering needed to be applied to the online dataset to make sure that no biased species observations would be used in our models. The filtering involved mainly: selection based on GBIF's basis of records ('HUMAN_OBSERVATION', 'LITERATURE', 'MATERIAL_SAMPLE', 'OBSERVATION', 'MATERIAL CITATION' kept), removal of observation duplicates, removal of observations without coordinates, removal of absence records, removal of observations with equal latitude and longitude, removal of observations identified as having corrupted coordinates, removal of observations older than 1970, removal of coordinates with less than four decimals, and removal of raster centroid datasets [46].

In total, the original observational dataset included 6'655'163 unique observations accurate to 11.1 meters for 4'250 species (see Table S2, Fig. S19a) and 30% of records from the Global Biodiversity Information (GBIF; https://doi.org/10.15468/dd.mb6jzt). This set was further filtered according to the prevalence of each species (or proportion of 100 m pixels occupied); i.e. species occurring in less than 30 pixels across the study area were removed. In total, the refined observational dataset included 3'167 species used in model calibration (see Fig. S19b, Table S3 for further description). It is important to note that for species with > 10'000 observations, we sampled randomly without replacement a subset of 10'000 observations for better computation efficiency [47,48]. Additionally, an independent and unbiased test dataset, reporting the empirical and distributional range of our 3'167 plant species over the European Alps, was constructed from expert-based information available in the Flora Alpina (FA)

[44] and the extraction of the 5-95th percentiles elevation values of each species (see Fig. S20 for more information)

Environmental Data

Climate

Four bioclimatic variables, known to have major ecophysiological effects on plant life [19,49,50], were extracted from the Climatologies at High resolution for the Earth's Land Surfaces Areas (CHELSA v2.1) portal [51] (http://chelsa-climate.org/) and using the *chelsa-cmip6* python library [52]: growing degree days (GDD), annual precipitation (BIO12), temperature (BIO4) and precipitation seasonality (BIO15). These predictors were obtained at 1 km resolution, for current climate (time period 1981-2010), and future climate (2041-2060 and 2071-2090) for 14 CMIP6 scenarios; i.e., two Shared Socioeconomic Pathways emissions (SSP245, SSP585) – an updated equivalent of the Representative Concentration Pathways (RCPs) 4.5 and 8.5 respectively – and seven Global Climate Model scenarios (GCM; GFDL-ESM4, MIROC6, AWI-CM-1-1-MR, EC-Earth3, IPSL-CM6A-LR, INM-CM5-0, MPI-ESM1-2-LR).

Soil

We derived soil property layers at a 100 m resolution over the study area by mapping ecological indicator values (EIVs) [53,54] in space following the method described in [54]. First, we obtained plant EIVs for 4'489 species from Flora Alpina [44] and retained 2 different EIVs to characterize the local edaphic conditions: soil nitrogen (EIV-N) and soil substrate composition (EIV-G). EIVs of the Flora Alpina are ordinal variables consisting of 3 classes each (low = 1, medium = 2, high = 3) and associated estimated species frequency in the classes (not occurring = 0, rare = 0.5, frequent = 1). For each species, we calculated the average EIV value weighted by the frequency of the species in the EIV classes. Second, EIV values were combined to our unfiltered observational dataset (i.e. 6'655'163 observations of 4'250 plant species) mapped on a 100 m grid. We removed duplicate observations of individual species per grid cell. Grid cells including at least ten species were then kept to calculate, for each EIV, a mean value across all species' EIV values per grid cell. EIV models were then calibrated from these cells at 100 m spatial resolution with Random Forest [55] using seven predictors representing topography and geology (see Table S4 for the list of predictors), and were predicted across the study area at a 100 m grain. EIV models were evaluated using Spearman's rank correlation tests by partitioning the data into training (80%) and evaluation (20%) sets following 2 approaches: (i) five-fold split-sampling of the data and (ii) five-fold spatial block cross-validation [56] using five strata assigned across 25 regional clusters across the Alps. All generated EIV soil property layers showed excellent evaluations with Spearman $r > 0.82$ (see Table S5). The generated EIV soil property layers are proxies of soil nitrogen and substrate composition, and have been shown to be excellent predictors of plant species distribution in SDMs [54,57]. The obtained EIV soil property layers were proxies of soil nitrogen (NITROGEN) and substrate composition (CALCAREOUS%). It is important to note that given the unavailability of future predicted soil information, we considered current and future soil unchanged.

Land cover

Land cover (LC) is also known to have a strong influence on species distributions [5,58–60]. Therefore, two LC change scenarios were obtained from the EU funded ALARM-ECOCHANGE and VOLANTES-HERCULES projects [61–64] at 1 km resolution, each including 6 original (grassland, forest, built-up, cropland, permanent crops, others) and 10 reclassified LC categories respectively (pasture, semi-natural vegetation, forest, built-up, permanent crops, irrigated/non-irrigated arable land, recently abandoned

pasture/arable land, others; see Table S6). While current LC is derived from the CORINE 2000 classification [65], future LC includes two emissions scenarios consistent with the SSP245 and SSP585 [66,67], namely, B1-SEDG (Sustainable European Development Goal) and A2-BAMBU (Business-As-Might-Be-Usual), both available for the time period 2041-2060 (for ECOCHANGE and HERCULES) and 2071-2090 (for ECOCHANGE only).

Correlation

All predictors were projected to the standard Lambert Azimuthal Equal Area projection for Europe (EPSG:3035), and continuous current predictors (climate and soil) showed a Pearson's inter-correlations of $|r| < 0.7$ (see Fig. S21), as suggested when model projections outside the calibration range are involved [50].

Observer bias correction

Bias covariate correction

Our observational dataset originated from a range of different sources which often lack sampling design, therefore, a strong geographic bias towards Switzerland and France was present in our refined observational dataset (see Fig. S19). To correct for this bias, three potential bias covariates were generated over the study area [48,68]: the target group observation density, distance to roads and cities. (i) The target group observation density was constructed, based on the original observational dataset (6'655'163 observations for 4'250 species), at 100 m across the study area (see Fig. S19a). Distance to roads (ii) and to cities (iii) were generated based on OpenStreetMap (https://www.openstreetmap.org). All roads and cities of the study region were extracted from this source and converted into two binary 100 m grids. Distances to roads and cities were then independently calculated with GDAL and python 3.6 (function *gdal.ComputeProximity*, https://gdal.org/). All bias covariates were projected to EPSG:3035, after square root transformation [68,69]. It is important to note that all bias covariates were weakly correlated with climate and soil; i.e. Pearson's $|r| < 0.3$ (see Fig. S21). Environmental effects were therefore hardly masked by observer-bias effects during model calibration [69].

Environmental bias correction

Before data collection, appropriate sampling design should be environmentally stratified [70–73]. Sampling frequencies in environmental space may in fact still remain skewed if species observations are not initially sampled according to an environmental stratification. Therefore to additionally address the environmental bias in the sampling design of our refined observational dataset (see Fig. S22), a recent corrective method, based on environmental stratified resampling of the observational dataset, was implemented before model calibration using the R function wsl.ebc [48]. Environmental bias correction (EBC) corrects potential environmental bias in the design of an observational dataset, by artificially sub-sampling original species observations based on a chosen number of environmental clusters over the study area. Using the R function clValid (R package clValid) [74] and following recommendations of [48], we set the number of environmental clusters to 20, i.e. summarizing not too precisely the environmental space of the study area, yet, large enough to account for the its environmental complexity. Within the function wsl.ebc, we set the different parameters as follows: (i) ras = the four current climate and two soil predictors; (ii) pportional = TRUE, i.e. to apply EBC with a proportional stratified sampling design (or EBCp); (iii) plog = TRUE, i.e. EBCp should adopt a log consensus; (iv) sp.specific = TRUE, i.e. EBCp applies only for species subject to an environmental bias;

(v) sp.cor = 0.5, i.e. correlation threshold of the environmental bias; (vi) keep.bias = TRUE, i.e. per species and after EBC applies, the number of observations in the densest original cluster is reset to that of the densest corrected cluster; (vii) filter = FALSE; i.e. the observations are not filtered according to the ras resolution. In total, EBC applied to 1248 species. The resulting corrected observations and their environmental frequencies (before and after EBC) may be found in Fig. S23.

Species distribution models

Calibration

For each species, model calibrations were done at 100 m resolution, by including current climate/LC (1 km), soil (100 m) as well as our bias predictors (100 m), and were calibrated twice i.e., one model per categorical LC.

We used a special type of presence-only SDMs, namely point-process models (PPMs). Point-process models (PPMs) were employed for our analyses. PPMs are statistical models that may be used to analyze species presence-only data. Model output represents the intensity of the expected number of species occurrences per unit area, that is modelled as a log-linear function of the environmental covariates [68,75]. At location s, the intensity $\lambda(s)$ is thus given by:

$$\ln\lambda(\mathrm{s}) = \mathbf{x}(\mathrm{s})'\boldsymbol{\beta} \qquad \text{[eqn 1]}$$

where $\boldsymbol{x}(s)$ is the vector of the p environmental covariates, and $\boldsymbol{\beta} = \{\beta_1, \dots, \beta_p\}$ is the vector of the corresponding regression coefficients. Given the vector of n observations $\boldsymbol{s}_P = \{s_1, \dots, s_n\}$, PPMs are fitted via maximum likelihood, and the parameters are found to maximise [76]:

$$l(\boldsymbol{\beta};\ \boldsymbol{s}_P) = \sum_{i=1}^{n} \ln \lambda(s_i) \ - \ \int_A \lambda(s)\, ds \qquad \text{[eqn 2]}$$

where the integral of the intensity over the entire study area **A** has to be approximated numerically. Such approximation requires the introduction of 'quadrature points', a set of points at which the intensity function is evaluated. As discussed in detail in [68], these points are needed to approximate the integral. The likelihood can thus be approximated as:

$$l(\boldsymbol{\beta};\ \boldsymbol{s}_P) \approx \sum_{i=1}^{n} \ln \lambda(s_i) - \sum_{j=1}^{n+m} w_j \lambda(s_j) \qquad \text{[eqn 3]}$$

$$= \sum_{i=1}^{n+m} w_i \, (y_i \ln \lambda(s_i) - \lambda(s_i)\,) \qquad \text{[eqn 4]}$$

Where $\boldsymbol{s}_0 = \{s_{n+1}, \dots, s_{n+m}\}$ are the quadrature points and $\boldsymbol{w} = \{w_1, \dots, w_{n+m}\}$ the quadrature weights. Since this is the likelihood of a weighted Poisson regression, PPMs belong to the family of generalized linear models (GLMs) [77] and can be fitted using any package in **R** capable of fitting GLMs. We therefore used the basic function *glm*, and we calibrated our models as a 'down-weighted Poisson regression' (DWPR) [68] with second-order polynomials (except for categorical land cover), and elastic net regularization [78] for all covariates.

DWPR with elastic net was executed using the R package *glmnet* [79]. Elastic Net represents a type of regularization and variable selection mixing lasso and ridge regression approaches [78]. It penalizes non-relevant predictors that might lead to overfitting by shrinking their effects or removing them completely. Elastic net regularization requires two parameters: alpha (α), which sets the balance between lasso and ridge, and lambda (λ), which sets the penalty coefficient level. For each evaluation

fold, we set α to 0.5, and determined the optimal λ by testing 100 different values and selecting the one for which model fit performed best under a new 5-fold cross-validation (function *cv.glmnet*).

Quadrature points were sampled randomly without replacement across the study area over a 100 m regular mesh. Because log-likelihood convergence is model specific, we estimated for each PPM the appropriate number of quadrature points by running 10 repeated series of DWPR and gradually increasing the number of randomly sampled points from 5000 to 600'000 points following [68] (see Fig. S24). For weights implemented in model calibrations, small ones were assigned to observations (1e-06), and given a study area of 294'994 km^2, quadrature weights (QW) were calculated following [68]:

$$QW = study\ area\ (km^2)/quadrature\ points\ (n) \qquad \text{[eqn 5]}$$

Therefore, when n = 5000, $QW \approx 589.9$; n = 10'000, $QW \approx 29.5$; n = 20'000, $QW \approx 14.7$; n = 50'000, $QW \approx 5.9$; n = 100'000, $QW \approx 2.9$; n = 150'000, $QW \approx 1.9$; n = 200'000, $QW \approx 1.5$; n = 250'000, $QW \approx 1.2$; n = 400'000, $QW \approx 0.7$; n = 600'000, $QW \approx 0.5$.

Evaluation

We evaluated the predictive performance of each PPM against the Flora Alpina (FA) test dataset by using 5-fold spatial block split-sampling tests [56]. This approach involves preliminarily delineating independent spatial blocks to partition observations in geographic space. Here, for each species, we evenly partitioned its observations, quadrature points and Flora Alpina presences/absences into 10 blocks and combined them to 5 folds (see Fig. S25 for more details). PPM performance was then evaluated using Flora Alpina presences/absences of the left-out fold, and models performing poorly – i.e. concurrently having a True Skill Statistic (TSS) and Boyce index < 0.3 – were removed [80–82].

Projection

For each species, retained calibrated models were projected for current and future scenarios across the study area at 100 x 100 m resolution, by setting the three bias covariates to a constant value of zero for all cells to correct for the fitted observer bias [48,69]. Probabilistic projections were then averaged across CMIP6/LC scenarios to generate per species one current (year 2000) and four future habitat suitability maps (i.e. considering unlimited dispersal; 2050-SSP245, 2050-SSP585, 2080-SSP245 and 2080-SSP585). Each set of species maps were further processed (a) according to previous literature [83] and (b) with simple dispersal models [84–86], to generate four additional suitability maps considering (i) no dispersal and (ii) realistic dispersal respectively (1'711 species were kept).

When using species distribution models (SDMs), one major inconvenient, while identifying changes in the potential distribution of a species, is accounting for its dispersal limitations. Standard SDMs projections in future environmental conditions implicitly assume unlimited dispersal. Said differently, model predictions of future changes in the distribution of a species indirectly presume that the species can colonize any suitable environmental habitats/pixels regardless of its location. This is a problem as many geographic (physical barriers such as rivers, forests or mountains) and ecological features (species dispersal capacity) might impede the species from dispersing too far from its initial distribution. Therefore, the R package *MigClim* (function *MigClim.migrate*) [85,87] was for each species employed so that dispersal limitations could be considered within each of their future habitat suitability (HS) maps, i.e. generating four future HS maps considering 'realistic dispersal' (scenarios 2050-SSP245, 2050-SSP585, 2080-SSP245 and 2080-SSP585). To that end, the five original projected HS maps of all species (current and 'unlimited dispersal') were used concurrently with the seed dispersal distances available for 1'711 species [84]. Since *MigClim* can only process binary layers of presences/absences, HS probability maps of each species were converted to binary rasters using the best

TSS threshold (mean TSS threshold of the retained calibrated models). *MigClim* was run by setting the key parameters as follows:

(a) *dispKernel* considered a vector ***Pdisp***(x) of dispersal probabilities calculated with a negative exponential dispersal Kernel [86,88]:

$$Pdisp(x) = e^{-x/\Theta} \qquad \text{[eqn 6]}$$

where $\boldsymbol{x}$ is a vector of distances ranging from 100 meters (study resolution) to the maximum dispersal distance of the species in meters with a 100 meters' step, and $\boldsymbol{\Theta}$ the median dispersal distance of the species in meters.

(b) *barrier* considered a binary raster of physical barriers that was specific to each species type. Based on CORINE land cover 2000 [65], barriers were defined if the feature's area > 2 km^2. In total, three barrier layers were generated, i.e. for species subsisting in (1) open, (2) mixte and (3) forest habitats. Although all layers had common barriers (water, snow and glaciers), layer (1) additionally included forests, while layer (3) included every land cover class except forests.

(c) *barrierType* was defined as 'weak' (i.e. dispersal through pixel corners allowed).

(d) *lddFreq* defines a frequency percentage of long-distance dispersal (LDD) events. It was set to 0.01 (or 1%) [85,89].

(e) *lddMinDist* defines the LDD minimum distance. It was automatically set following the minimum value requirement of the *MigClim* user guide [87].

(f) *lddMaxDist* defines the LDD maximum distance. It was set according to each dispersal type following [89].

(g) *iniMatAge* stands for 'initial maturity age'. It was set to 2, which means that colonized cells may produce new propagules only after 2 model dispersal steps (or 2 years, i.e. once the plant hypothetically reached initial maturity).

(h) *propaguleProd* defines the probability of propagule production for each age between the initial maturity age and full maturity. It was set to a vector defined as c(0.01, 0.08, 0.5, 0.92), i.e. a simple sigmoid function generally known to represent plant growth [87,90].

(i) *replicateNb* defines the number of *MigClim* simulations. This was set to 3 to account for model stochasticity.

For each of the 1'711 species, the five original HS probability maps (current and 'unlimited dispersal') were intersected with (i) *MigClim* binary outputs and (ii) the original binary rasters. This provided new current HS maps informing concurrently on species occurrence probabilities and absences, which included four new future HS maps of (i) 'realistic' and (ii) 'unlimited dispersal' respectively. Furthermore, four additional future HS maps of 'no dispersal' were generated following [83]. To that end, the original current binary raster was intersected with the four new 'unlimited dispersal' HS maps, i.e. we only kept as suitable areas those concurrently occurring for present and future conditions. Finally, all final layers (i.e. 13 per species) were each aggregated by mean to a 1 km resolution, as stacked SDMs provide more meaningful predictions of species diversity when species distributions are aggreagated from high to lower resolution [19,57,91].

Multifaceted diversity and uniqueness

Diversity

For current and each of the 12 dispersal scenarios, spatial taxonomic, phylogenetic and functional diversity were calculated as abundance-based diversity with Hill numbers and their recent extensions [92–95].

Taxonomic. For each 13 scenarios, we generated a community matrix summarizing the absolute occurrence probabilities of the 1'711 species per pixel across the study area. For each matrix, TD was calculated as abundance-based species diversity based on Hill numbers [92] with the R package *hillR* (function *hill_taxa*) [96]. Here, we chose the order q = 1 (or the Shannon entropy $\boldsymbol{H}$), i.e. an average sensitivity of the calculated pixel diversity to species absolute occurrence probabilities.

Phylogenetic. Based on the detailed name list of our 1'711 modelled species (family, genus and species), a phylogenetic tree was computed using the R package *V.PhyloMaker* (function *phylo.maker*) [97]. *V.PhyloMaker* may generate large phylogenies for vascular plants based on updated versions of two plant mega-phylogenies [98,99]. These phylogenies were built based on fossil records, molecular data from GenBank (https://www.ncbi.nlm.nih.gov/genbank/) and phylogenetic data from the Open Tree of Life (https://tree.opentreeoflife.org/), including over 70 000 species of vascular plants. Using the phylogeny, PD was calculated for each community matrix based on extended Hill numbers to phylogenetic diversity (function *hill_phylo*) [93,96]. Same Hill order was here kept (q =1), i.e. phylogenetic diversity of each pixel was here calculated with the phylogenetic entropy $\boldsymbol{H}_{\mathrm{P}}$; a generalization of the Shannon entropy [95,100]. It is generally known that PD is not independent from TD [21,101]. Therefore, the residuals of a linear regression of TD on PD (quadratic terms included) were extracted to generate new layers of relative phylogenetic diversity (rPD) [102–104].

Functional. (i) Trait data was compiled from 33 individual sources comprising national data centers (e.g. InfoFlora, CBNA), European projects (e.g. OriginAlps, Fifth, Ecochange) and various sources from the literature and from collaborators (for a complete list, see Table S7). Mean plant height, leaf dry matter content, specific leaf area and leaf carbon to nitrogen ratio were extracted for our 1'711 species (i.e. 4'308 traits). In total, 1'344 species were missing at least one trait (~35% of total missing values). (ii) Missing information in trait databases is a chronic issue in ecological studies [105,106]. While removing species with absent information is considered a common practice [107,108], such practice is problematic if data are not missing taxonomically or phylogenetically at random (MCAR) [106,109]. An alternative imputation is preferred and strongly recommended when trait data are indeed missing at random (MAR) [107,108]. Our trait data had ~35% of missing values (2'536 measurements out of 6'844); i.e. an acceptable percentage under both MCAR and MAR assumptions [107,110]. We tested both assumptions by applying preliminary MCAR (*MissMech* R package) [111] and multiple-imputation tests (R package *mice*) [112] respectively, and found our missing data to follow rather the MAR than the MCAR assumption (see Fig. S26). We therefore substituted missing trait values by implementing the MAR imputation method (function *mice*, method *rf)*, which has demonstrated good performances of trait data imputation [107,108]. (iii) Trait values were normalized from 0 to 1 and Gower's distances were calculated thereof [113,114]. Based on the distance matrix, functional dendrograms were generated from different algorithms with the R package *cluster* (function *daisy)* [115]. We kept the functional tree whose cophenetic distance matrix was the most correlated with the initial distance matrix (UPGMA functional tree) [116]. Finally, based on a Mantel test using 9'999 randomizations (R package *vegan*, function *mantel*) [117], we found the functional dendrogram to express ~78% of the initial distance matrix ($r = 0.777$; *** *P-value* < 0.001) indicating a strong conservation of the original functional space. (iv) Using the obtained functional dendrogram, FD was calculated for each community matrix based on extended Hill numbers to functional diversity (function *hill_func*) [94,96]. Same Hill order was here kept (q =1), i.e. functional

diversity of each pixel was here calculated with a compromise index, i.e. at the interface between the functional attribute diversity and the weighted Gini-Simpson index [95,118,119]. As PD, FD is generally not independent from TD. Therefore, the residuals of a linear regression of TD on FD (quadratic terms included) were also extracted to generate new layers of relative functional diversity (rFD).

Uniqueness

Using same data resources, we calculated for each scenario weighted taxonomic (WE), phylogenetic (PE) and functional endemism (FE) across the study area. Using our phylogeny and functional dendrogram three types of endemism were calculated for each community matrix. (1) Weighted taxonomic endemism ***WE*** is defined as the species richness in one pixel divided by the sum of the species ranges [24]:

$$\mathrm{WE} = \sum_{t \in T} \frac{1}{R_t} \qquad \text{[eqn 7]}$$

where $\boldsymbol{R_t}$ represents the regional geographic range of species $\boldsymbol{t}$ (or number of pixels over the study area where its occurrence probabilities > 0). WE was calculated with the R package *phyloregion* (function *weighted_endemism)* [120]. (2) Weighted phylogenetic endemism ***PE*** is defined as the sum of branch length in one pixel divided by the regional range of each branch on the spanning path connecting a set of taxa to the root of a phylogenetic tree [25]:

$$\mathrm{PE} = \sum_{c \in C} \frac{L_c}{R_c} \qquad \text{[eqn 8]}$$

where $\boldsymbol{R_c}$ represents the regional geographic range of branch $\boldsymbol{c}$ (or number of pixels over the study area where the branch occurs), and $\boldsymbol{L_c}$ the length of branch $\boldsymbol{c}$. PE was calculated with the R package *phyloregion* (function *phylo_endemism)* [120]. (3) Weighted functional endemism ***FE*** was calculated based on our functional dendrogram with the same approach as PE:

$$\mathrm{FE} = \sum_{i \in I} \frac{L_i}{R_i} \qquad \text{[eqn 9]}$$

where $\boldsymbol{R_i}$ represents the regional geographic range of the functional branch $\boldsymbol{i}$ (or number of pixels over the study area where the branch occurs), and $\boldsymbol{L_i}$ the length of functional branch $\boldsymbol{i}$. FE was calculated with the R package *phyloregion* (function *phylo_endemism)* [120]. Relative phylogenetic and functional endemism (rPE and rFE) were generated following the same procedure and justifications as for rPD and rFD. Finally, we also calculated for each scenario phylogenetic (PR) and functional rarity (FR) across the study area following [121]. Using our functional dendrogram, functional rarity (***FR***) [27] was calculated for each community matrix (preliminary converted to relative abundance matrix as specified by [121] based on four distinct metrics using the R package *funrar* (function *funrar*) [121]: (1) scarcity, (2) geographical restrictiveness, (3) functional distinctiveness and (4) uniqueness. (1) Scarcity ($\boldsymbol{S_t}$) defines the local rarity of a species:

$$S_t = \exp\left(-NA_t \ln(2)\right) \qquad \text{[eqn 10]}$$

where $\boldsymbol{N}$ is the number of species and $\boldsymbol{A_t}$ the occurrence probability of species $\boldsymbol{t}$ in one pixel. (2) Restrictiveness ($\boldsymbol{GR_t}$) defines the regional rarity of a species:

$$GR_t = 1 - \frac{R_t}{R_{total}} \qquad \text{[eqn 11]}$$

where $\boldsymbol{R_t}$ is the number of pixels where species $\boldsymbol{t}$ occurs and $\boldsymbol{R_{total}}$ the total number of pixels of the study area. (3) Functional distinctiveness ($\boldsymbol{D_t}$) defines the uncommonness of traits of a species compared to other species' traits in one pixel weighted by their absolute occurrence probabilities:

$$D_t = \frac{\sum_{j=1,j\neq t}^{N} d_{tj}A_j}{\sum_{j=1,j\neq t}^{N} A_j} \qquad \text{[eqn 12]}$$

where $\boldsymbol{d_{tj}}$ is the functional dissimilarity between species $\boldsymbol{t}$ and species $\boldsymbol{j}$, $\boldsymbol{N}$ and $\boldsymbol{A_j}$ the number of species and the absolute occurrence probability of species $\boldsymbol{j}$ in the pixel respectively. (4) Functional uniqueness ($\boldsymbol{U_t}$) is the functional distance of a species $\boldsymbol{t}$ to its closest neighbor in a given region:

$$U_t = \min(d_{tj}) \qquad \text{[eqn 13]}$$

where $\boldsymbol{d_{tj}}$ is the functional dissimilarity between species $\boldsymbol{t}$ and species $\boldsymbol{j}$. Scarcity, restrictiveness, functional distinctiveness and uniqueness were calculated for each species and pixel. Unlike scarcity and distinctiveness, restrictiveness and uniqueness are only calculated per species. Therefore, to obtain values per species and pixel, each species' relative abundances across the study area were weighted by its level of restrictiveness and uniqueness respectively. Total scarcity ($\boldsymbol{S_{total}}$), restrictiveness ($\boldsymbol{GR_{total}}$), functional distinctiveness ($\boldsymbol{D_{total}}$) and uniqueness ($\boldsymbol{U_{total}}$) were each obtained over the study area by averaging values across species. As suggested by [121], each spatial metric were normalized from 0 to 1 and functional rarity was obtained by calculating the average:

$$FR = \frac{S_{total} + GR_{total} + D_{total} + U_{total}}{4} \qquad \text{[eqn 14]}$$

Finally, using the same relative abundance matrices and our phylogeny, 13 phylogenetic rarity ($\boldsymbol{PR}$) [28] were calculated over the study region with the same approach as functional rarity using the R package *funrar* (function *funrar*) [121].

System Conservation Planning

Zonation

Conservation prioritizations were run using the conservation planning software Zonation 4.0 [122,123]. Zonation ranks cells of a considered region from high to low conservation values, based on both the irreplaceability and complementarity of input ecological features [124,125]. Zonation computes the conservation values of all conservation units (in this case raster cells) based on the distribution of all features, and iteratively removes cells with the lowest conservation values until all are removed [126]. For each current and dispersal outcome, we ran multifaceted-based prioritizations to maximize concurrently the representation of species, phylogenetic, and functional distinctiveness. For this, our aggregated species distributions were used as Zonation features, and each species layer was weighted by the sum of its phylogenetic and functional uniqueness.

We ran 52 prioritization scenarios (see Table S8 for parameters) i.e., for each current and dispersal scenario outcome (n=13), accounting for two prioritization allocation approaches (*optimal reserve selection* and *reserve network expansion*) and using the *core-area Zonation* (CAZ) and *additive benefit function* (ABF) prioritization algorithms. The 'selection' approach identifies the highest priority areas on the entire landscape without accounting for the current configuration of PAs. The 'expansion' approach considers the current reserve network of the Alps including PAs designated as IUCN I-II and Natura 2000 categories. In this approach, areas outside of PAs are ranked allowing for identification of

the highest priorities outside the current PAs network that best complement protected biodiversity. For the main regional/transnational conservation strategies (Fig. 4), the 'expansion' approach was used together with the CAZ algorithm, which assigns conservation values by maximizing regional diversity and its complementarity i.e., by minimizing the extinction of features and protecting the worst-off ones (those with very little distribution remaining). For the main local/national conservation strategies (Fig. 3), the 'expansion' approach was used together with the ABF algorithm, which assigns conservation values by maximizing local diversity hotspots and their complementarity i.e., by minimizing the extinction of local multifaceted richness. In total, 52 maps of conservation priority were generated (see Table S9 for summary).

Post-analysis

In line with the post-2020 global framework of the Convention on Biological Diversity (CBD), we chose the top 20% of the current, 2050 and 2080 *reserve network expansion* simulations (Fig. 4), to correctly project a conservation overlap that would extent the present PAs network to ~30% of the European Alps' area. For each percentage of expanding PAs over the study region, we calculated the cumulative representation of species, phylogenetic and functional branch occurrence probabilities, of their range, and of species functional/phylogenetic rarity (Fig. S1a-b). For this purpose, aggregated SDM occurrence probabilities of each species were employed and each phylogenetic and functional branch's spatial occurrence probabilities were calculated following [127]. While the probability of occurrence of terminal branches are inferred from that of the species, the probability of occurrence of internal branches in each cell is calculated as:

$$B_{ij} = 1 - \prod_{n-1}^{m}(1 - P_{nj}) \qquad \text{[eqn 15]}$$

where $\boldsymbol{B}_{ij}$ is the probability of an internal branch $\boldsymbol{i}$ in cell $\boldsymbol{j}$, $\boldsymbol{m}$ the number of descendant species originating from the internal branch and $\boldsymbol{P}_{nj}$ the probability of descendent species $\boldsymbol{n}$ to occur in cell $\boldsymbol{j}$. Therefore, for each percentage of expanding PAs over the study region, we calculated the cumulative representation of (1) species, (2) phylogenetic and (3) functional branch occurrence probabilities, of (4) species, (5) phylogenetic and (6) functional branch distributional range, and of species (7) functional and (8) phylogenetic rarity. (2) The cumulative representation of phylogenetic diversity (PD) was calculated following [127]:

$$PD\ (\%) = \frac{1}{\sum_{i=1}^{k} L_i} \cdot \sum_{i=1}^{k}\left[\left(L_i \cdot \frac{\sum_{j=1}^{q} B_{ij}}{\sum_{j=1}^{Q} B_{ij}}\right)\right] \times 100 \qquad \text{[eqn 16]}$$

where $\boldsymbol{k}$ is the number of branches of the phylogenetic tree, $\boldsymbol{q}$ the cells covered by PAs (%), $\boldsymbol{Q}$ the total number of cells in the landscape, $\boldsymbol{B}_{ij}$ the probability of occurrence of branch $\boldsymbol{i}$ in cell $\boldsymbol{j}$ and $\boldsymbol{L}$ is the length of branch $\boldsymbol{i}$. (3) The cumulative representation of functional diversity (FD) was calculated the same way but using the functional branches information. (1) Based on the previous equation, the cumulative representation of species diversity (TD) was calculated as:

$$TD\ (\%) = \frac{1}{N} \cdot \sum_{i=1}^{N}\left[\frac{\sum_{j=1}^{q} A_j}{\sum_{j=1}^{Q} A_{ij}}\right] \times 100 \qquad \text{[eqn 17]}$$

where $\boldsymbol{N}$ is the total number of species, $\boldsymbol{q}$ the cells covered by PAs (%), $\boldsymbol{Q}$ the total number of cells in the landscape, $\boldsymbol{A}_{ij}$ the probability of occurrence of species $\boldsymbol{i}$ in cell $\boldsymbol{j}$. (4) The cumulative representation of species endemism (WE) was calculated following [26]:

$$WE\ (\%) = \frac{1}{N} . \sum_{i=1}^{N} \frac{s_i}{S_i} \times 100 \qquad \text{[eqn 18]}$$

where $\boldsymbol{N}$ is the total number of species, $\boldsymbol{s}_i$ the number of cells covered by PAs (%) where the species occurs, and $\boldsymbol{S}_i$ the total number of cells where the species occurs. (5) The cumulative representation of phylogenetic endemism (PE) was calculated following [26]:

$$PE\ (\%) = \frac{1}{\sum_{i=1}^{k} L_i} . \sum_{i=1}^{k} \left[L_i \ . \ \frac{e_i}{E_i} \right] \times 100 \qquad \text{[eqn 19]}$$

where $\boldsymbol{k}$ is the number of branches of the tree, $\boldsymbol{e}_i$ the number of cells covered by PAs (%) where the branch occurs, $\boldsymbol{E}_i$ the total number of cells where the branch occurs, and $\boldsymbol{L}$ is the length of branch $\boldsymbol{i}$. (6) The cumulative representation of functional endemism (FE) was calculated the same way but using the functional branches information. (7) The cumulative representation of species functional rarity (FR) was adapted from [eqn 1] and calculated as:

$$FR\ (\%) = \frac{1}{N} . \sum_{i=1}^{N} \left[\frac{\sum_{j=1}^{q} R_{ij}}{\sum_{j=1}^{Q} R_{ij}} \right] \times 100 \qquad \text{[eqn 20]}$$

where $\boldsymbol{N}$ is the total number of species, $\boldsymbol{q}$ the cells covered by PAs (%), $\boldsymbol{Q}$ the total number of cells in the landscape, and $\boldsymbol{R}_{ij}$ the functional rarity of species $\boldsymbol{i}$ in cell $\boldsymbol{j}$. (8) The cumulative representation of species phylogenetic rarity (PR) was calculated the same way but using the phylogenetic rarity of each species.

Additionally, we define 'Expanded PAs' as the 2- or 3-time overlap of the top 20% reserve expansion of current, 2050 and 2080 prioritizations (Fig. 4). The 95th elevation values percentile was calculated per species by extracting the values of a Digital Elevation Model (DEM) with species observations (Fig. 2; see also Fig. S20). Finally, percentage of gains and losses (Fig. 2) were calculated for each species based on their range, that is the number of pixels of the study region that the species occupies, as follows:

$$\frac{|Range_{future} - Range_{current}|}{Range_{current}} \times 100 \qquad \text{[eqn 21]}$$

References and Notes

1. European Commission. *EU Biodiversity Strategy for 2030, Bringing nature back into our lives, https://ec.europa.eu/info/sites/default/files/communication-annex-eu-biodiversity-strategy-2030_en.pdf*. (2020).
2. European Commission. The European Green Deal, https://eur-lex.europa.eu/resource.html?uri=cellar:b828d165-1c22-11ea-8c1f-01aa75ed71a1.0002.02/DOC_1&format=PDF. (2019).
3. Chemini, C. & Rizzoli, A. Land use change and biodiversity conservation in the Alps. *Journal of Mountain Ecology* 1–7 (2003).
4. Sabatini, F. M. *et al.* Global patterns of vascular plant alpha diversity. *Nature Communications* **13**, (2022).
5. Chauvier, Y. *et al.* Influence of climate, soil, and land cover on plant species distribution in the European Alps. *Ecological Monographs* **91**, 1–14 (2021).
6. Smyčka, J. *et al.* Tempo and drivers of plant diversification in the European mountain system. *Nature Communications* **13**, (2022).
7. Kraaijenbrink, P. D. A., Stigter, E. E., Yao, T. & Immerzeel, W. W. Climate change decisive for Asia's snow meltwater supply. *Nature Climate Change* **11**, 591–597 (2021).
8. Sorg, A., Bolch, T., Stoffel, M., Solomina, O. & Beniston, M. Climate change impacts on glaciers and runoff in Tien Shan (Central Asia). *Nature Climate Change* **2**, 725–731 (2012).
9. Tuanmu, M. N. *et al.* Climate-change impacts on understorey bamboo species and giant pandas in China's Qinling Mountains. *Nature Climate Change* **3**, 249–253 (2013).
10. Rumpf, S. B. *et al.* From white to green Snow cover loss and increased vegetation productivity in the European Alps. *Science* **1122**, 1119–1122 (2022).
11. Mastrotheodoros, T. *et al.* More green and less blue water in the Alps during warmer summers. *Nature Climate Change* **10**, 155–161 (2020).
12. Pepin, N. *et al.* Elevation-dependent warming in mountain regions of the world. *Nature Climate Change* **5**, 424–430 (2015).
13. Bálint, M. *et al.* Cryptic biodiversity loss linked to global climate change. *Nature Climate Change* **1**, 313–318 (2011).
14. Rumpf, S. B. *et al.* Range dynamics of mountain plants decrease with elevation. *Proceedings of the National Academy of Sciences* **115**, 1848–1853 (2018).
15. Alexander, J. M. *et al.* Lags in the response of mountain plant communities to climate change. *Global Change Biology* **24**, 563–579 (2018).
16. Benayas, J. M. R., Martins, A., Nicolau, J. M. & Schulz, J. J. Abandonment of agricultural land: An overview of drivers and consequences. *CAB Reviews* **2**, (2007).
17. Elsen, P. R., Monahan, W. B. & Merenlender, A. M. Global patterns of protection of elevational gradients in mountain ranges. *Proceedings of the National Academy of Sciences of the United States of America* **115**, 6004–6009 (2018).
18. Joppa, L. N. & Pfaff, A. High and far: Biases in the location of protected areas. *PLoS ONE* **4**, 1–6 (2009).
19. Thuiller, W. *et al.* Are different facets of plant diversity well protected against climate and land cover changes? A test study in the French Alps. *Ecography* **37**, 1254–1266 (2014).
20. Dullinger, S. *et al.* Extinction debt of high-mountain plants under twenty-first-century climate change. *Nature Climate Change* **2**, 619–622 (2012).
21. Devictor, V. *et al.* Spatial mismatch and congruence between taxonomic, phylogenetic and functional diversity: The need for integrative conservation strategies in a changing world. *Ecology Letters* **13**, 1030–1040 (2010).
22. Faith, D. P. Conservation evaluation and phylogenetic diversity. *Biological Conservation* **61**, 1–10 (1992).
23. Petchey, O. & Gaston, K. J. Functional diversity (FD), species richness and community composition. *Ecology Letters* **5**, 402–411 (2002).

24. Crisp, M. D., Laffan, S., Linder, H. P. & Monro, A. Endemism in the Australian flora. *Journal of Biogeography* **28**, 183–198 (2001).
25. Rosauer, D., Laffan, S. W., Crisp, M. D., Donnellan, S. C. & Cook, L. G. Phylogenetic endemism: A new approach for identifying geographical concentrations of evolutionary history. *Molecular Ecology* **18**, 4061–4072 (2009).
26. Pollock, L. J., Thuiller, W. & Jetz, W. Large conservation gains possible for global biodiversity facets. *Nature* **546**, 141–144 (2017).
27. Violle, C. *et al.* Functional rarity: the ecology of outliers. *Trends in Ecology & Evolution* **32**, 356–367 (2017).
28. Grenié, M. *et al.* Functional rarity of coral reef fishes at the global scale: Hotspots and challenges for conservation. *Biological Conservation* **226**, 288–299 (2018).
29. Lenoir, J., Gégout, J. C., Marquet, P. A., De Ruffray, P. & Brisse, H. A significant upward shift in plant species optimum elevation during the 20th century. *Science* **320**, 1768–1771 (2008).
30. Chen, I. C., Hill, J. K., Ohlemüller, R., Roy, D. B. & Thomas, C. D. Rapid range shifts of species associated with high levels of climate warming. *Science* **333**, 1024–1026 (2011).
31. Elsen, P. R. & Tingley, M. W. Global mountain topography and the fate of montane species under climate change. *Nature Climate Change* **5**, 772–776 (2015).
32. Pauli, H. *et al.* Recent plant diversity changes on Europe's mountain summits. *Science* **336**, 353–355 (2012).
33. Steinbauer, M. J. *et al.* Accelerated increase in plant species richness on mountain summits is linked to warming. *Nature* **556**, 231 (2018).
34. Dirnböck, T., Essl, F. & Rabitsch, W. Disproportional risk for habitat loss of high-altitude endemic species under climate change. *Global Change Biology* **17**, 990–996 (2011).
35. Rumpf, S. B. *et al.* Extinction debts and colonization credits of non-forest plants in the European Alps. *Nature Communications* **10**, 1–9 (2019).
36. Alexander, J. M., Diez, J. M. & Levine, J. M. Novel competitors shape species' responses to climate change. *Nature* **525**, 515–518 (2015).
37. Gottfried, M. *et al.* Continent-wide response of mountain vegetation to climate change. *Nature Climate Change* **2**, 111–115 (2012).
38. Norberg, J., Urban, M. C., Vellend, M., Klausmeier, C. A. & Loeuille, N. Eco-evolutionary responses of biodiversity to climate change. *Nature Climate Change* **2**, 747–751 (2012).
39. Hermoso, V. *et al.* The EU Biodiversity Strategy for 2030: Opportunities and challenges on the path towards biodiversity recovery. *Environmental Science and Policy* **127**, 263–271 (2022).
40. Thompson, J. D. *Plant Evolution in the Mediterranean: Insights for conservation*. (2020). doi:10.1093/oso/9780198835141.001.0001
41. Comes, H. P. The Mediterranean Region: A Hotspot for Plant Biogeographic Research. *The New Phytologist* **164**, 11–14 (2004).
42. Hewitt, G. M. Genetic consequences of climatic oscillations in the Quaternary. *Philosophical Transactions of the Royal Society B: Biological Sciences* **359**, 183–195 (2004).
43. Permanent Secretariat of the Alpine Convention. *Alpine Convention - The Alps eight countries, a single territory. Herzog-Friedrich-Straße 15, A-6020 Innsbruck, Austria Branch*. (2009).
44. Aeschimann, D., Lauber, K., Moser, D. M. & Theurillat, J. P. *Flora alpina: ein Atlas sämtlicher 4500 Gefässpflanzen der Alpen.* (2004).
45. Chauvier, Y. *et al.* gbif.range - An R package to generate species range maps based on ecoregions and a user-friendly GBIF wrapper. *Envidat* 1-12. doi: 10.16904/envidat.352 (2022). doi:10.16904/envidat.352
46. Zizka, A. *et al.* CoordinateCleaner: Standardized cleaning of occurrence records from

biological collection databases. *Methods in Ecology and Evolution* **2019**, 1–8 (2019).
47. Thuiller, W. *et al.* Combining point-process and landscape vegetation models to predict large herbivore distributions in space and time—A case study of Rupicapra rupicapra. *Diversity and Distributions* **24**, 352–362 (2018).
48. Chauvier, Y. *et al.* Novel methods to correct for observer and sampling bias in presence-only species distribution models. *Global Ecology and Biogeography* **30**, 2312–2325 (2021).
49. Randin, C. F., Vuissoz, G., Liston, G. E., Vittoz, P. & Guisan, A. Introduction of Snow and Geomorphic Disturbance Variables into Predictive Models of Alpine Plant Distribution in the Western Swiss Alps. *Arctic, Antarctic, and Alpine Research* **41**, 347–361 (2009).
50. Brun, P. *et al.* Model complexity affects species distribution projections under climate change. *Journal of Biogeography* **47**, 130–142 (2020).
51. Karger, D. N. *et al.* Climatologies at high resolution for the earth's land surface areas. *Scientific Data* **4**, 1–20 (2017).
52. Karger, D. N., Chauvier, Y. & Zimmermann, N. E. chelsa-cmip6 1.0: A python package to create high resolution bioclimatic variables based on CHELSA V2.1 and CMIP6 data. *Ecography (under review)*
53. Landolt, E. *et al. Flora indicativa. Ökologische Zeigerwerte und biologische Kennzeichen zur Flora der Schweiz und der Alpen*. (2010).
54. Descombes, P. *et al.* Spatial modelling of ecological indicator values improves predictions of plant distributions in complex landscapes. *Ecography* **43**, 1448–1463 (2020).
55. Breiman, L. Random Forests. *Machine Learning* **45**, 5–32 (2001).
56. Roberts, D. R. *et al.* Cross-validation strategies for data with temporal, spatial, hierarchical, or phylogenetic structure. *Ecography* **40**, 913–929 (2017).
57. Chauvier, Y. *et al.* Resolution in species distribution models shapes spatial patterns of plant multifaceted diversity. *Ecography* **2022**, e05973 (2022).
58. Thuiller, W., Araujo, M. B. & Lavorel, S. Do we need land-cover data to model species distributions in Europe? *Journal of Biogeography* **31**, 353–361 (2004).
59. Titeux, N. *et al.* Biodiversity scenarios neglect future land-use changes. *Global change biology* **22**, 2505–2515 (2016).
60. Randin, C. F. *et al.* Monitoring biodiversity in the Anthropocene using remote sensing in species distribution models. *Remote Sensing of Environment* **239**, 111626 (2020).
61. Dendoncker, N., Bogaert, P. & Rounsevell, M. A statistical method to downscale aggregated land use data and scenarios. *Journal of Land Use Science* **1**, 63–82 (2006).
62. Rounsevell, M. D. A. *et al.* A coherent set of future land use change scenarios for Europe. *Agriculture, Ecosystems and Environment* **114**, 57–68 (2006).
63. Stürck, J. *et al.* Simulating and delineating future land change trajectories across Europe. *Regional Environmental Change* **18**, 733–749 (2018).
64. Schulp, C. J. E., Levers, C., Kuemmerle, T., Tieskens, K. F. & Verburg, P. H. Mapping and modelling past and future land use change in Europe's cultural landscapes. *Land Use Policy* **80**, 332–344 (2019).
65. Bossard, M., Feranec, J. & Otahel, J. *CORINE Land Cover technical Guide - Addendum 2000. EEA Technical Report* (2000).
66. Spangenberg, J. H. Integrated scenarios for assessing biodiversity risks. *Sustainable Development* **15**, i–i (2007).
67. Collins, M. *et al.* Long-term Climate Change: Projections, Com- mitments and Irreversibility. in *Climate Change 2013: The Physical Science Basis. Contribution of Working Group I to the Fifth Assessment Report of the Intergovernmental Panel on Climate Change [Stocker, T.F., D. Qin, G.-K. Plattner, M. Tignor, S.K. Allen, J. Boschung, A. Nauels, Y. Xia,* (Cambridge University Press, Cambridge, United Kingdom and New York, NY, USA., 2013).

68. Renner, I. W. *et al.* Point process models for presence-only analysis. *Methods in Ecology and Evolution* **6**, 366–379 (2015).
69. Warton, D. I., Renner, I. W. & Ramp, D. Model-based control of observer bias for the analysis of presence-only data in ecology. *PLoS ONE* **8**, e79168 (2013).
70. Mohler, C. L. Effect of sampling pattern on estimation of species distributions along gradients. *Vegetatio* **54**, 97–102 (1983).
71. Austin, M. P. & Heyligers, P. C. Vegetation survey design for conservation: Gradsect sampling of forests in North-eastern New South Wales. *Biological Conservation* **50**, 13–32 (1989).
72. Hirzel, A. & Guisan, A. Which is the optimal sampling strategy for habitat suitability modelling. *Ecological Modelling* **157**, 331–341 (2002).
73. Albert, C. H. *et al.* Sampling in ecology and evolution - bridging the gap between theory and practice. *Ecography* **33**, 1028–1037 (2010).
74. Brock, G., Pihur, V., Datta, S. & Datta, S. clValid, an R package for cluster validation. *Journal of Statistical Software* (2011). doi:10.18637/jss.v025.i04
75. Warton, D. I. & Shepherd, L. C. Poisson point process models solve the 'pseudo-absence problem' for presence-only data in ecology. *Annals of Applied Statistics* **4**, 1383–1402 (2010).
76. Cressie, N. A. C. *Statistics for spatial data*. (1993). doi:10.1002/9781119115151
77. McCullagh, P. Generalized linear models. *European Journal of Operational Research* **16**, 285–292 (1984).
78. Zou, H. & Hastie, T. Regression and variable selection via the elastic net. *Journal of the Royal Statistical Society: Series B (Statistical Methodology)* **67**, 301–320 (2005).
79. Friedman, J., Hastie, T. & Tibshirani, R. Regularization Paths for Generalized Linear Models via Coordinate Descent. *J Stat Softw* **33**, 1–22 (2010).
80. Boyce, M. S., Vernier, P. R., Nielsen, S. E. & Schmiegelow, F. K. A. Evaluating resource selection functions. *Ecological Modelling* **157**, 281–300 (2002).
81. Allouche, O., Tsoar, A. & Kadmon, R. Assessing the accuracy of species distribution models: Prevalence, kappa and the true skill statistic (TSS). *Journal of Applied Ecology* **43**, 1223–1232 (2006).
82. Hirzel, A. H., Le Lay, G., Helfer, V., Randin, C. & Guisan, A. Evaluating the ability of habitat suitability models to predict species presences. *Ecological Modelling* **199**, 142–152 (2006).
83. Thuiller, W., Lavorel, S., Araújo, M., Sykes, M. & Prentice, C. Climate change threats to plant diversity in Europe. *Proceedings of the National Academy of Sciences of the United States of America* **102**, 8245–8250 (2005).
84. Vittoz, P. & Engler, R. Seed dispersal distances: A typology based on dispersal modes and plant traits. *Botanica Helvetica* **117**, 109–124 (2007).
85. Engler, R. & Guisan, A. MigClim: Predicting plant distribution and dispersal in a changing climate. *Diversity and Distributions* **15**, 590–601 (2009).
86. Zurell, D. *et al.* Benchmarking novel approaches for modelling species range dynamics. *Global change biology* **22**, 2651–2664 (2016).
87. Engler, R., Hordijk, W. & Guisan, A. The MIGCLIM R package - seamless integration of dispersal constraints into projections of species distribution models. *Ecography* **35**, 872–878 (2012).
88. Sutherland, G. D., Harestad, A. S., Price, K. & Lertzman, K. P. Scaling of natal dispersal distances in terrestrial birds and mammals. *Ecology and Society* **4**, (2000).
89. Engler, R. *et al.* Predicting future distributions of mountain plants under climate change: Does dispersal capacity matter? *Ecography* **32**, 34–45 (2009).
90. Liu, J. H. *et al.* Simulation of crop growth, time to maturity and yield by an improved sigmoidal model. *Scientific Reports* **8**, 6–11 (2018).
91. Thuiller, W., Pollock, L. J., Gueguen, M. & Münkemüller, T. From species distributions to

meta-communities. *Ecology Letters* **18**, 1321–1328 (2015).
92. Hill, M. O. Diversity and Evenness: A Unifying Notation and Its Consequences. *Ecology* **54**, 427–432 (1973).
93. Chao, A., Chiu, C. H. & Jost, L. Phylogenetic diversity measures based on Hill numbers. *Philosophical Transactions of the Royal Society B: Biological Sciences* **365**, 3599–3609 (2010).
94. Chiu, C. H. & Chao, A. Distance-based functional diversity measures and their decomposition: A framework based on hill numbers. *PLoS ONE* **9**, (2014).
95. Chao, A., Chiu, C. H. & Jost, L. Unifying species diversity, phylogenetic diversity, functional diversity, and related similarity and differentiation measures through hill numbers. *Annual Review of Ecology, Evolution, and Systematics* **45**, 297–324 (2014).
96. Li, D. hillR: taxonomic, functional, and phylogenetic diversity and similarity through Hill Numbers. *The Journal of Open Source Software* **3**, 1041 (2018).
97. Jin, Y. & Qian, H. V.PhyloMaker: an R package that can generate very large phylogenies for vascular plants. *Ecography* **42**, 1353–1359 (2019).
98. Zanne, A. E. *et al.* Three keys to the radiation of angiosperms into freezing environments. *Nature* **506**, 89–92 (2014).
99. Smith, S. A. & Brown, J. W. Constructing a broadly inclusive seed plant phylogeny. *American Journal of Botany* **105**, 302–314 (2018).
100. Allen, B., Kon, M. & Bar-Yam, Y. A new phylogenetic diversity measure generalizing the shannon index and its application to phyllostomid bats. *American Naturalist* **174**, 236–243 (2009).
101. Forest, F. *et al.* Preserving the evolutionary potential of floras in biodiversity hotspots. *Nature* **445**, 757–760 (2007).
102. Pavoine, S., Gasc, A., Bonsall, M. B. & Mason, N. W. H. Correlations between phylogenetic and functional diversity: Mathematical artefacts or true ecological and evolutionary processes? *Journal of Vegetation Science* **24**, 781–793 (2013).
103. Pardo, I. *et al.* Spatial congruence between taxonomic, phylogenetic and functional hotspots: true pattern or methodological artefact? *Diversity and Distributions* **23**, 209–220 (2017).
104. Thuiller, W. *et al.* Productivity begets less phylogenetic diversity but higher uniqueness than expected. *Journal of Biogeography* **47**, 44–58 (2020).
105. Májeková, M. *et al.* Evaluating Functional diversity: Missing trait data and the importance of species abundance structure and data transformation. *PLoS ONE* **11**, 1–17 (2016).
106. Nakagawa, S. & Freckleton, R. P. Missing inaction: the dangers of ignoring missing data. *Trends in Ecology and Evolution* **23**, 592–596 (2008).
107. Penone, C. *et al.* Imputation of missing data in life-history trait datasets: Which approach performs the best? *Methods in Ecology and Evolution* **5**, 1–10 (2014).
108. Johnson, T. F., Isaac, N. J. B., Paviolo, A. & González-Suárez, M. Handling missing values in trait data. *Global Ecology and Biogeography* **00**, 1–12 (2020).
109. Taugourdeau, S., Villerd, J., Plantureux, S., Huguenin-Elie, O. & Amiaud, B. Filling the gap in functional trait databases: Use of ecological hypotheses to replace missing data. *Ecology and Evolution* **4**, 944–958 (2014).
110. Madley-Dowd, P., Hughes, R., Tilling, K. & Heron, J. The proportion of missing data should not be used to guide decisions on multiple imputation. *Journal of Clinical Epidemiology* **110**, 63–73 (2019).
111. Jamshidian, M., Jalal, S. & Jansen, C. Missmech: An R package for testing homoscedasticity, multivariate normality, and missing completely at random (MCAR). *Journal of Statistical Software* **56**, 1–31 (2014).
112. van Buuren, S. & Groothuis-Oudshoorn, K. mice: Multivariate imputation by chained equations in R. *Journal of Statistical Software* **45**, 1–67 (2011).
113. Pavoine, S., Vallet, J., Dufour, A.-B., Gachet, S. & Daniel, H. On the challenge of treating

various types of variables: application for improving the measurement of functional diversity. *Oikos* **118**, 391–402 (2009).
114. Maire, E., Grenouillet, G., Brosse, S. & Villéger, S. How many dimensions are needed to accurately assess functional diversity? A pragmatic approach for assessing the quality of functional spaces. *Global Ecology and Biogeography* **24**, 728–740 (2015).
115. Maechler, M., Rousseeuw, P., Struyf, A., Hubert, M. & Hornik, K. Cluster: cluster analysis basics and extensions. *R package version* **1**, 56 (2019).
116. Mouchet, M. *et al.* Towards a consensus for calculating dendrogram-based functional diversity indices. *Oikos* **117**, 794–800 (2008).
117. Oksanen, J. *et al.* Package 'vegan'. Community ecology package, version, 2.0-9. 1–295 (2013).
118. Walker, B., Kinzig, A. & Langridge, J. Plant Attribute Diversity, Resilience, and Ecosystem Function: The Nature and Significance of Dominant and Minor Species. *Ecosystems* **2**, 95–113 (1999).
119. Guiasu, R. C. & Guiasu, S. The weighted Gini-Simpson index: Revitalizing an old index of biodiversity. *International Journal of Ecology* **2012**, (2012).
120. Daru, B. H., Farooq, H., Antonelli, A. & Faurby, S. Endemism patterns are scale dependent. *Nature Communications* **11**, 1–11 (2020).
121. Grenié, M., Denelle, P., Tucker, C. M., Munoz, F. & Violle, C. funrar: An R package to characterize functional rarity. *Diversity and Distributions* **23**, 1365–1371 (2017).
122. Moilanen, A. Landscape Zonation, benefit functions and target-based planning: Unifying reserve selection strategies. *Biological Conservation* **134**, 571–579 (2007).
123. Lehtomäki, J. & Moilanen, A. Methods and workflow for spatial conservation prioritization using Zonation. *Environmental Modelling and Software* **47**, 128–137 (2013).
124. Pollock, L. J. *et al.* Protecting Biodiversity (in All Its Complexity): New Models and Methods. *Trends in Ecology and Evolution* **35**, 1119–1128 (2020).
125. O'Connor, L. M. J. *et al.* Balancing conservation priorities for nature and for people in Europe. *Science* **373**, 856–860 (2021).
126. Moilanen, A. *et al.* Zonation–Spatial conservation planning methods and software. Version 4. User Manual, 290. (2014).
127. Pollock, L. J. *et al.* Phylogenetic diversity meets conservation policy: small areas are key to preserving eucalypt lineages. *Philosophical Transactions of the Royal Society B: Biological Sciences* **370**, 20140007–20140007 (2015).

Acknowledgments: We thank P. Descombes for providing the soil predictors, L. Boulangeat for the trait measurements, J. Renaud for the help on cleaning the species data and taxonomy, and all various contributors for sharing numerous datasets of species observations and traits, and for having made possible the large-scale scope of this study. We particularly thank Info Flora and the Conservatoire Botanique National Alpin, for their continuous effort in collecting and cleaning plant data across Switzerland and the French Alps. This work was supported by the ANR-SNF bilateral project OriginAlps, with grant numbers 310030L_170059 (Y.C., N.E.Z) and ANR-16-CE93-004 (W.T., S.L.). WT also acknowledges the French Biodiversity Agency for financial support and the HorizonEurope NaturaConnect project.

Author contributions: Conceptualization: Y.C., L.J.P., N.E.Z., W.T.; Methodology: Y.C., L.J.P., W.T.; Software: Y.C., P.H.V., D.N.K.; Investigation: Y.C.; Visualization: Y.C.; Formal analysis: Y.C.; Funding acquisition: N.E.Z., S.L., W.T.; Supervision: N.E.Z., W.T.; Writing – original draft: Y.C.; Writing – review & editing: Y.C., L.J.P., P.H.V., D.N.K., L.P., S.L., N.E.Z., W.T.

Competing interests: The authors declare that they have no competing interests.

Data and materials availability: All data, code, and materials supporting the findings of this study are available in the EnviDat repository https://doi.org/10.16904/envidat.371.

Appendix:

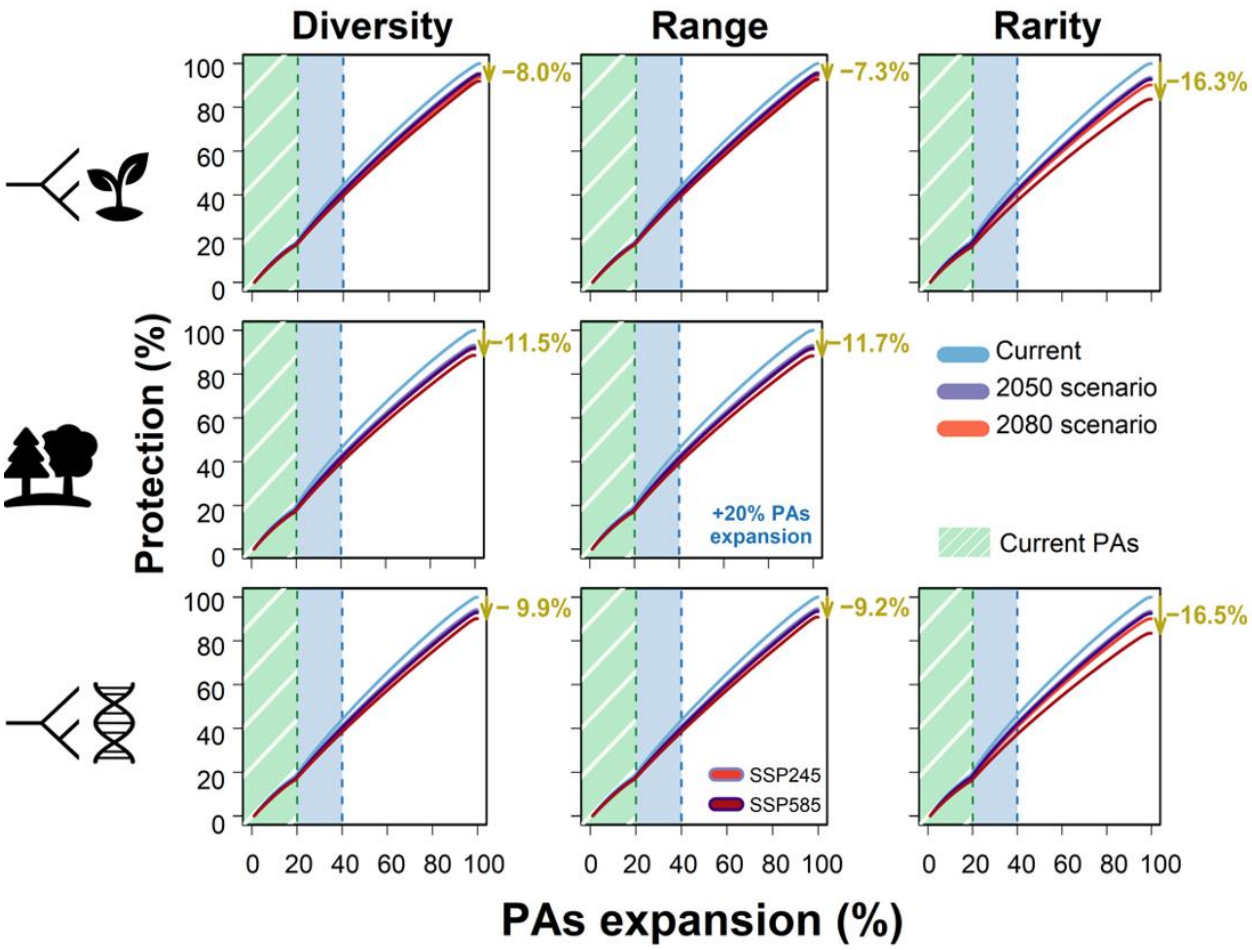

Figure S1a. Current and future protected areas (PAs) network cumulative expansion in the European Alps when maximizing local diversity for realistic plant dispersal. First, second and third row depict the functional, taxonomic, and phylogenetic dimension, respectively. Panels describe the cumulated protection of plant multifaceted diversity and uniqueness in function of the reserve network expansion (% of the study region) for each current and future conservation simulation. Yellow percentages display the amount of feature loss between the current and 2080 prioritization. Current PAs of the European Alps cover ~20% of the study region and are displayed in striped green. Results of expanding the reserve network by 20% are displayed over the panels in blue.

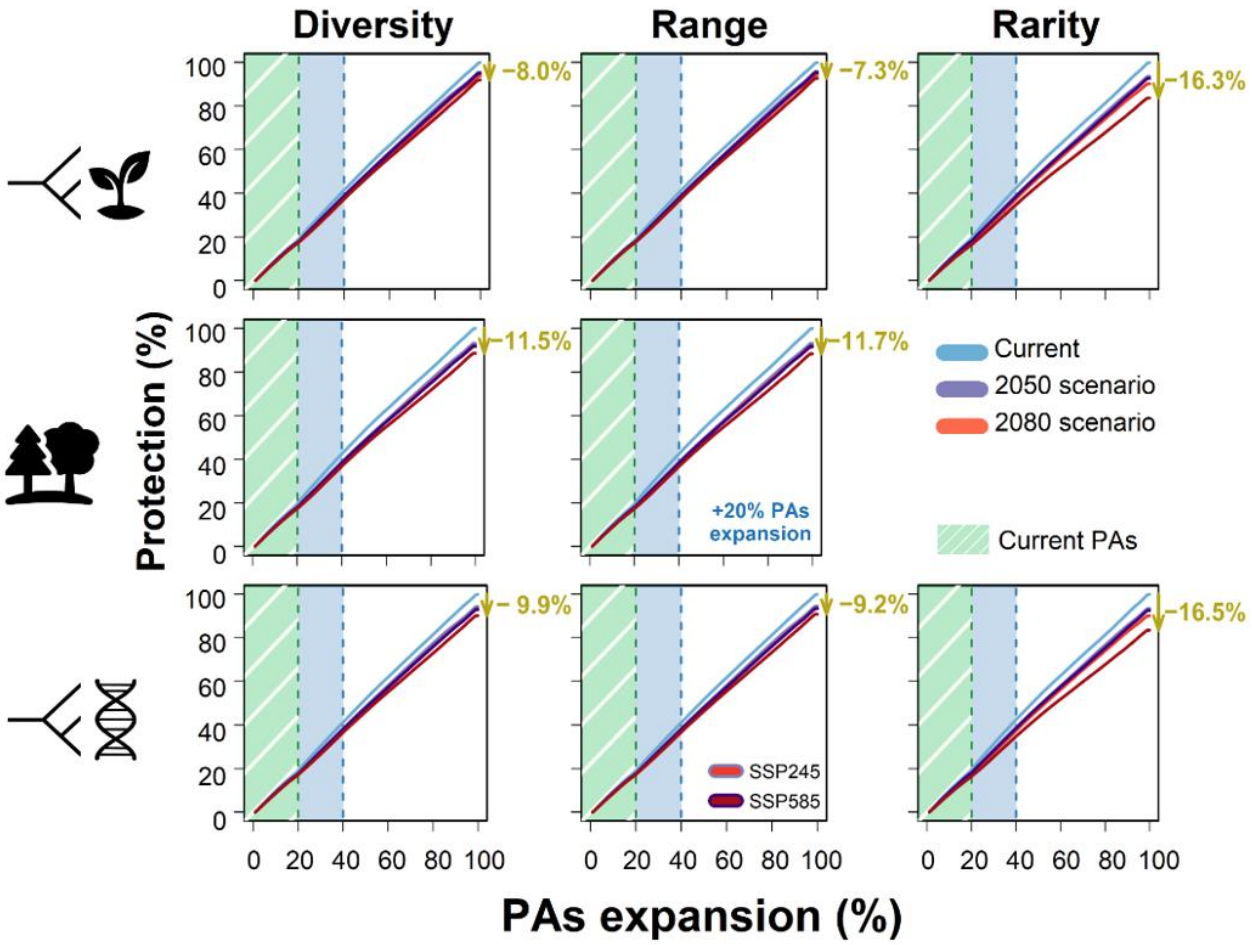

Figure S1b. Current and future protected areas (PAs) network cumulative expansion in the European Alps when maximizing regional diversity for realistic plant dispersal.

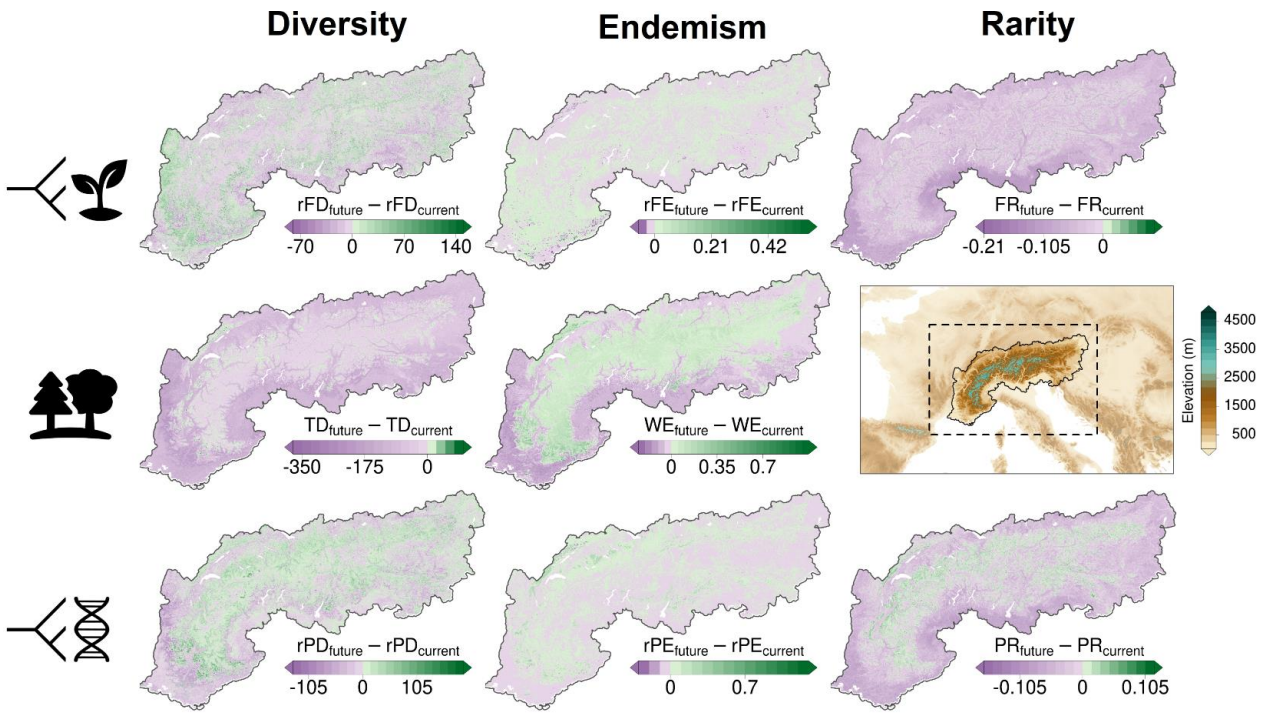

Figure S2a. Change in multifaceted diversity and uniqueness by 2050 for SSP585 and realistic plant dispersal.

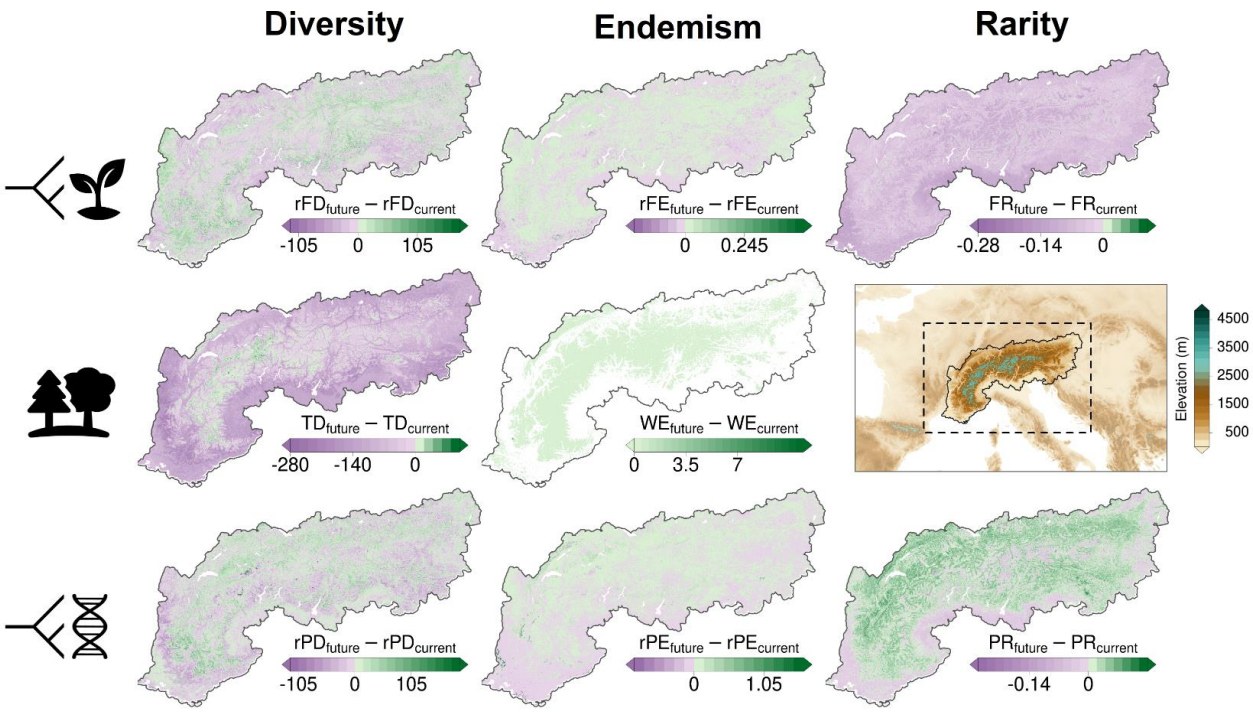

Figure S2b. Change in multifaceted diversity and uniqueness by 2080 for SSP245 and realistic plant dispersal.

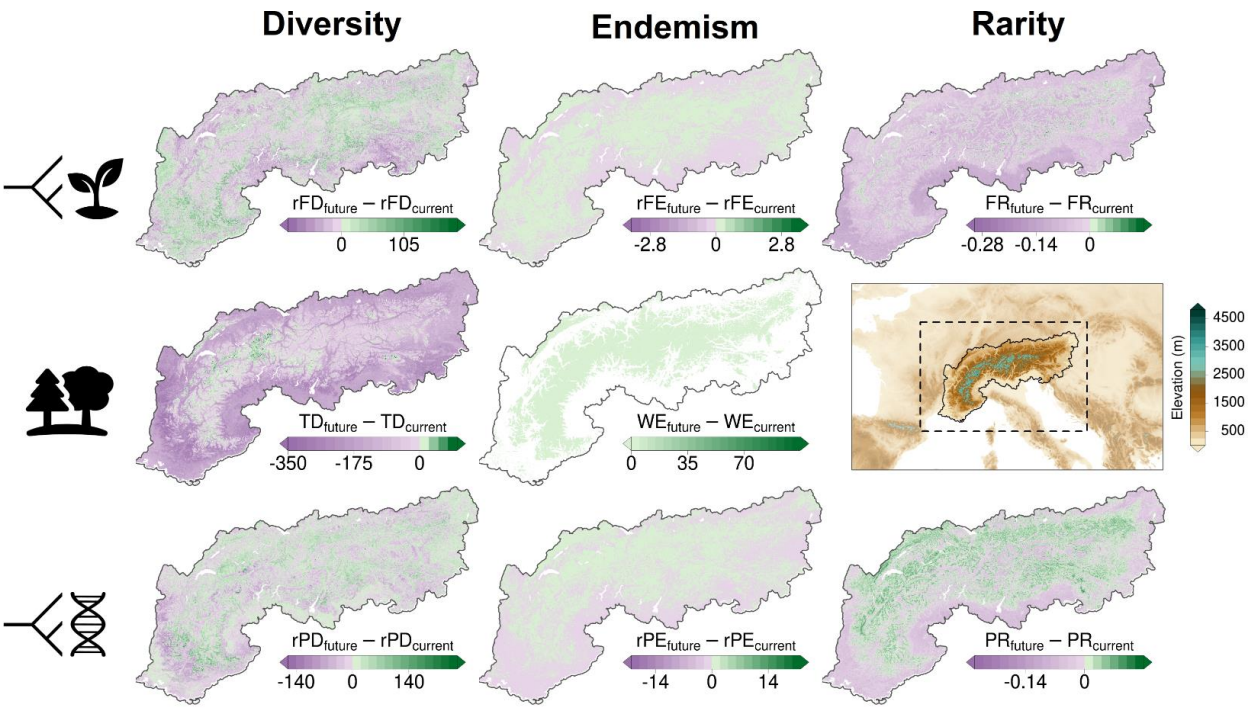

Figure S2c. Change in multifaceted diversity and uniqueness by 2080 for SSP585 and realistic plant dispersal.

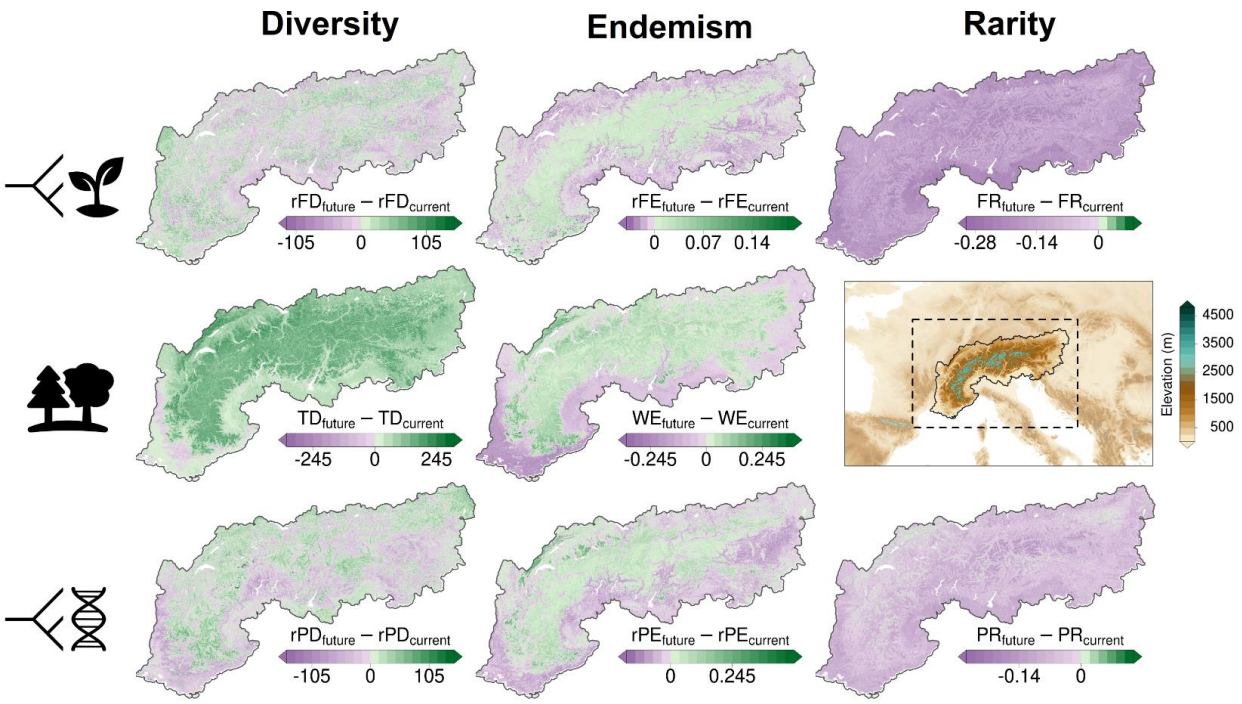

Figure S2d. Change in multifaceted diversity and uniqueness by 2050 for SSP245 and unlimited plant dispersal.

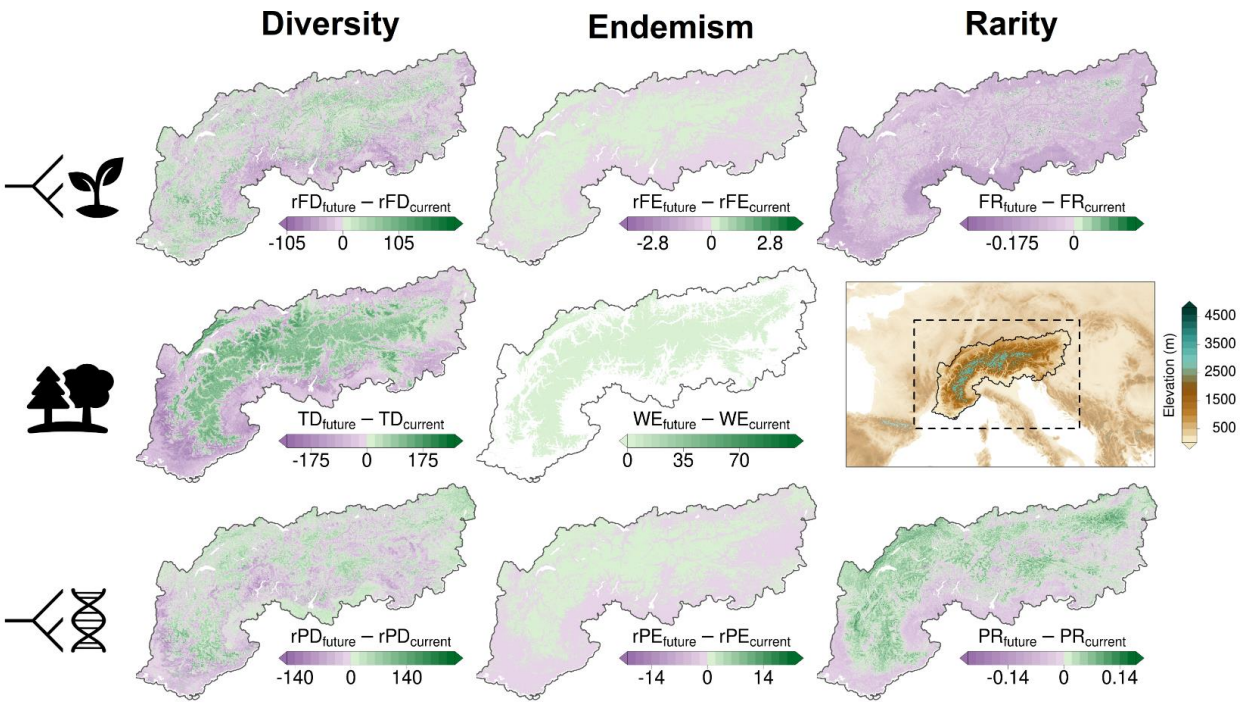

Figure S2e. Change in multifaceted diversity and uniqueness by 2080 for SSP585 and unlimited plant dispersal.

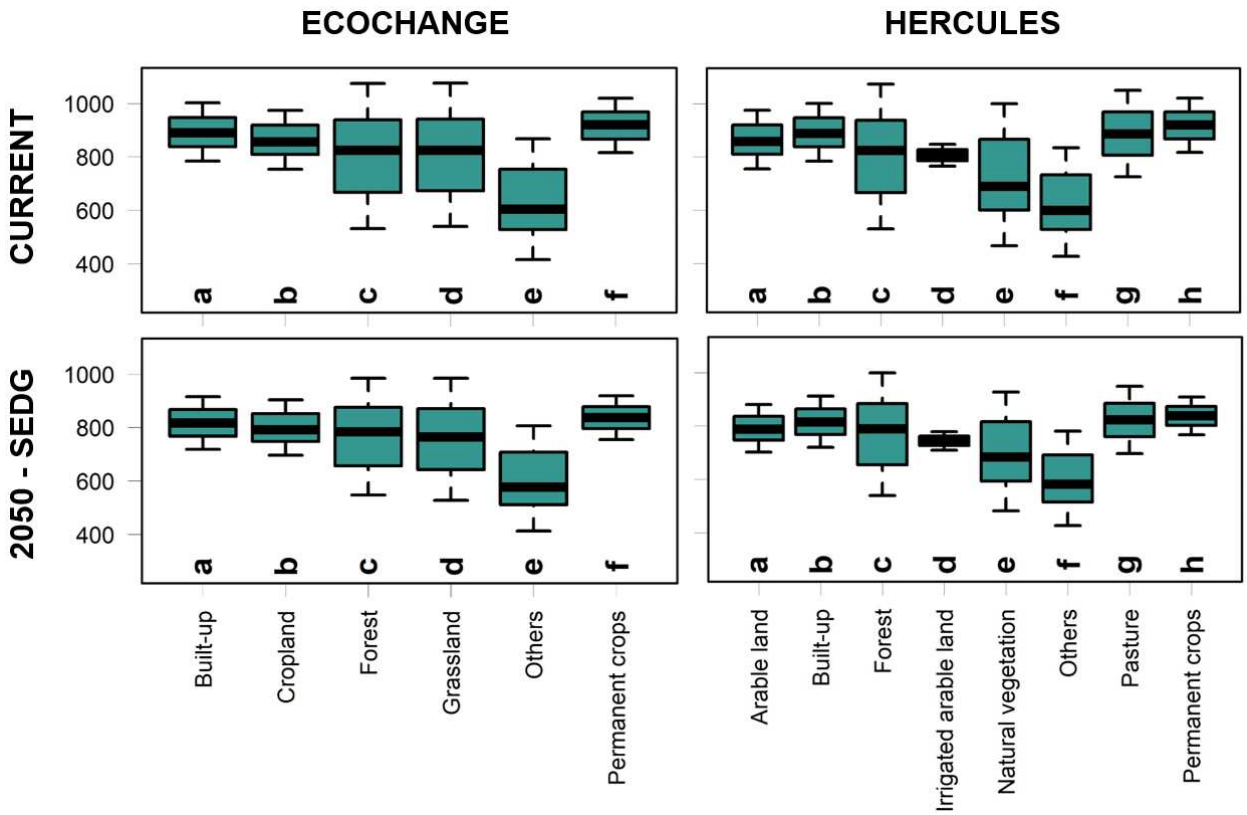

Figure S3. Plant species richness distribution by land cover type for two land cover products (ALARME-ECOCHANGE and VOLANTES-HERCULES) and timelines (current and by 2050 for the SEDG/SSP245 scenario). Kruskal-Wallis tests were here applied for each panel (****p*-value < .001 for all): Kruskal-Wallis X^2 = 36'256.01, 49'156.6, 32'335.8 and 41'398.6 (upper-left, -right, lower-left and -right, respectively). All pairwise comparisons were run with post-hoc Dunn tests and displayed following a letter-based representation (**p*-value > .05).

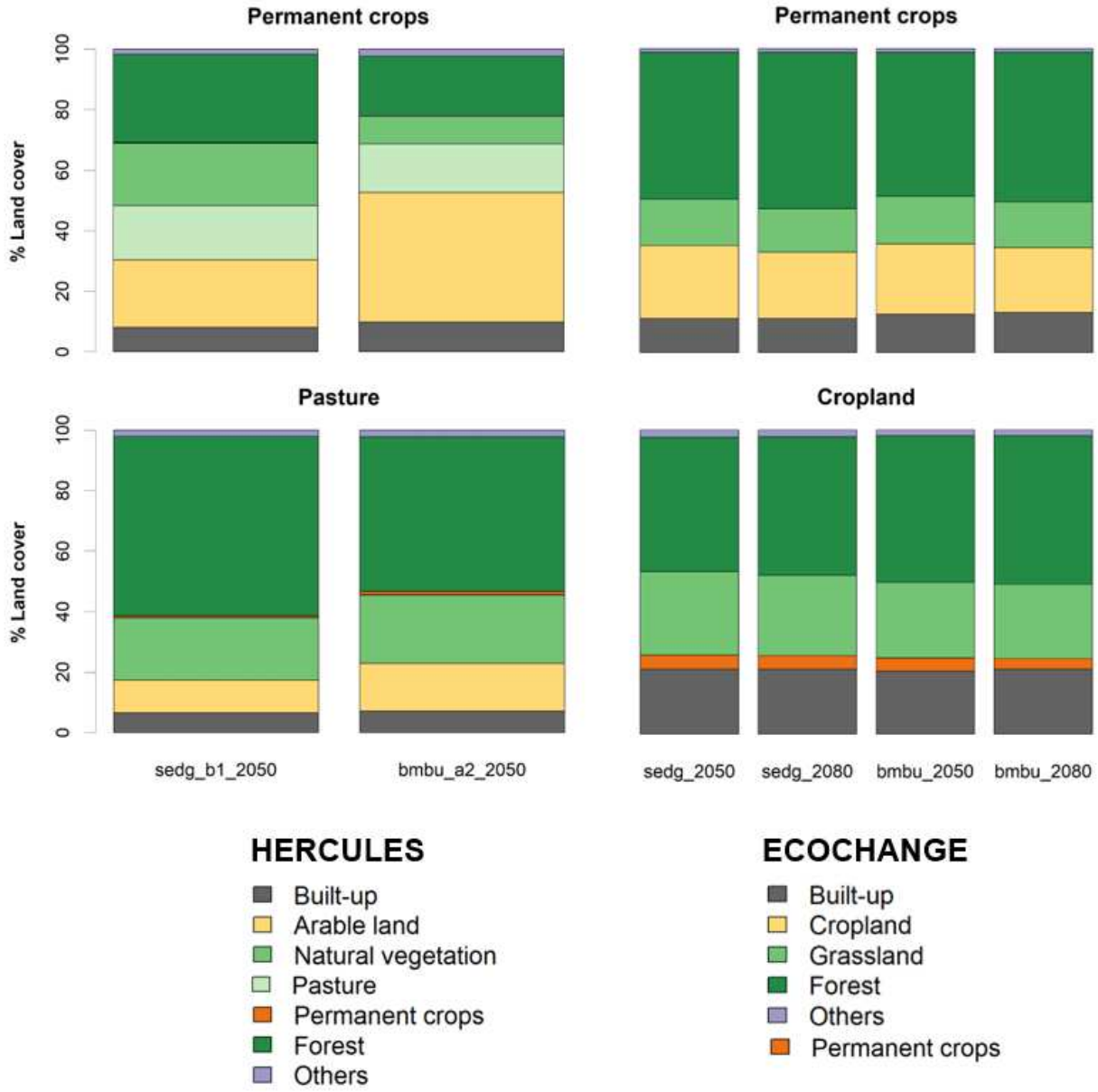

Figure S4. Land use change (%) for different types of agricultural land cover abandonment (Permanent crops, Pasture and Cropland), for VOLANTES-HERCULES (left panels) and ALARME-ECOCHANGE (right panels), and their associated carbon scenarios (by 2050 and 2080 for SEDG/SSP245 and BMBU/SSP585 scenario). For each future scenario, land use change (%) was calculated as the pixel proportion of new land cover types succeeding previous permanent crops, pasture or cropland.

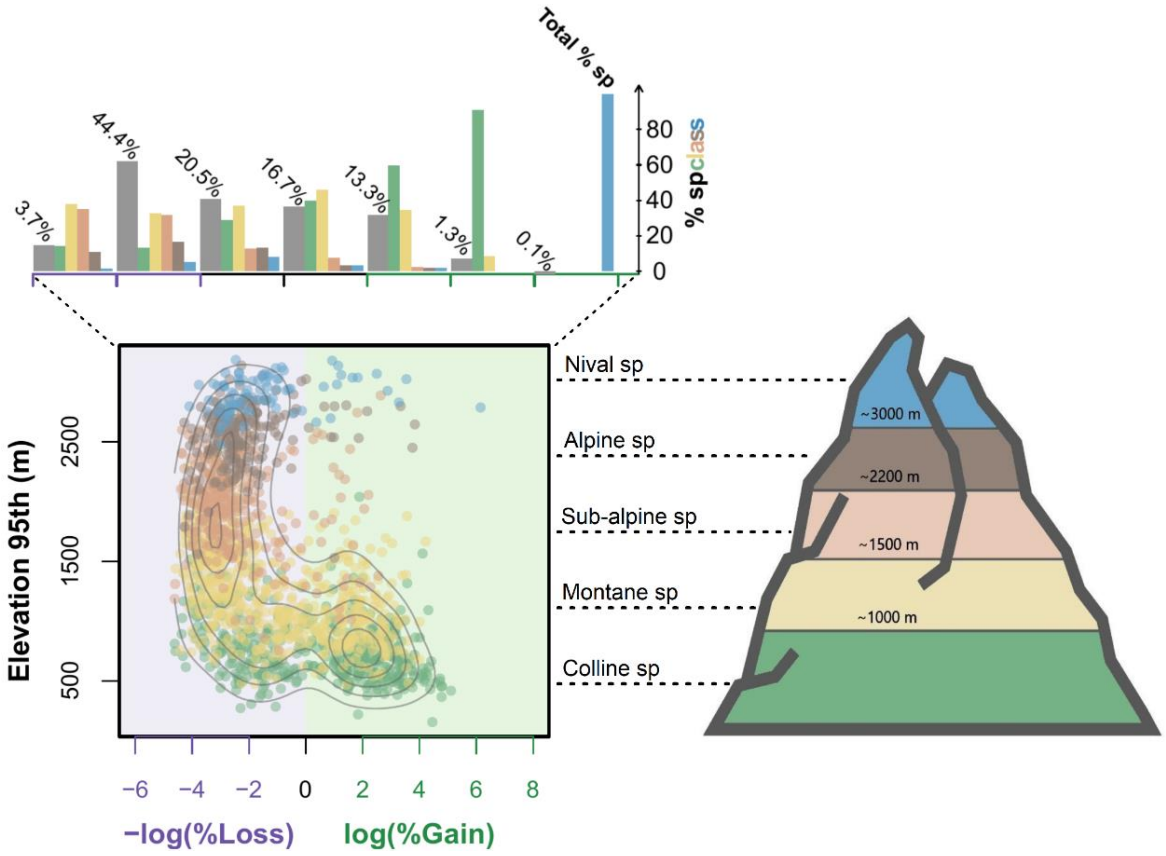

Figure S5a. Species range shifts by 2050 for SSP585 and realistic plant dispersal.

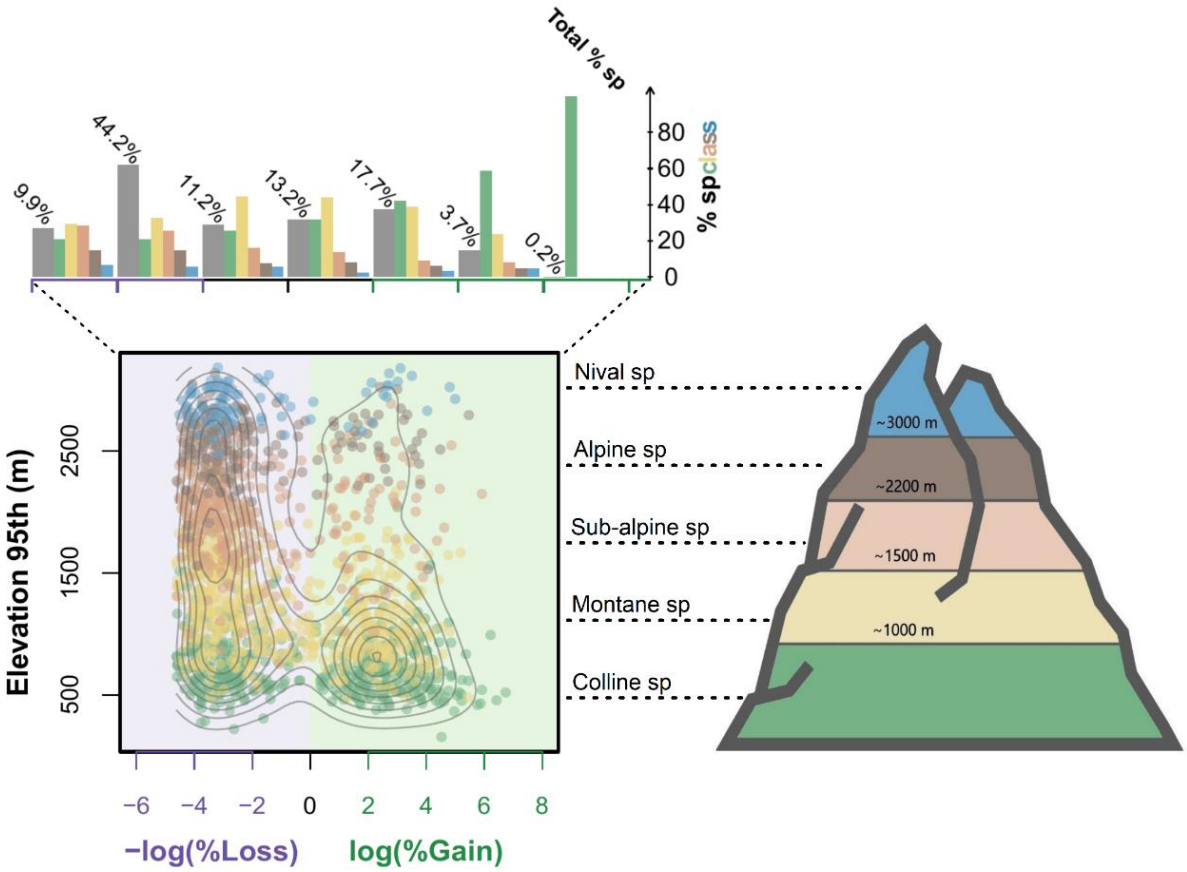

Figure S5b. Species range shifts by 2080 for SSP245 and realistic plant dispersal.

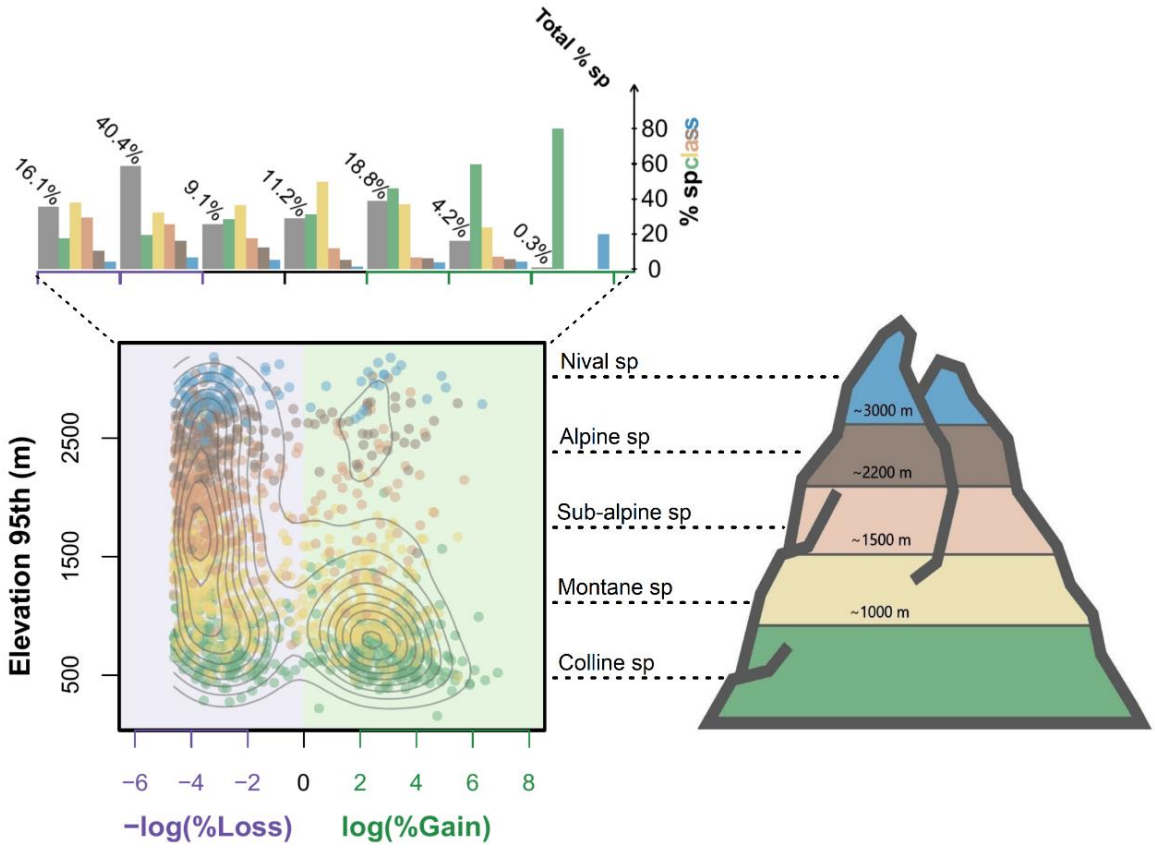

Figure S5c. Species range shifts by 2080 for SSP585 and realistic plant dispersal.

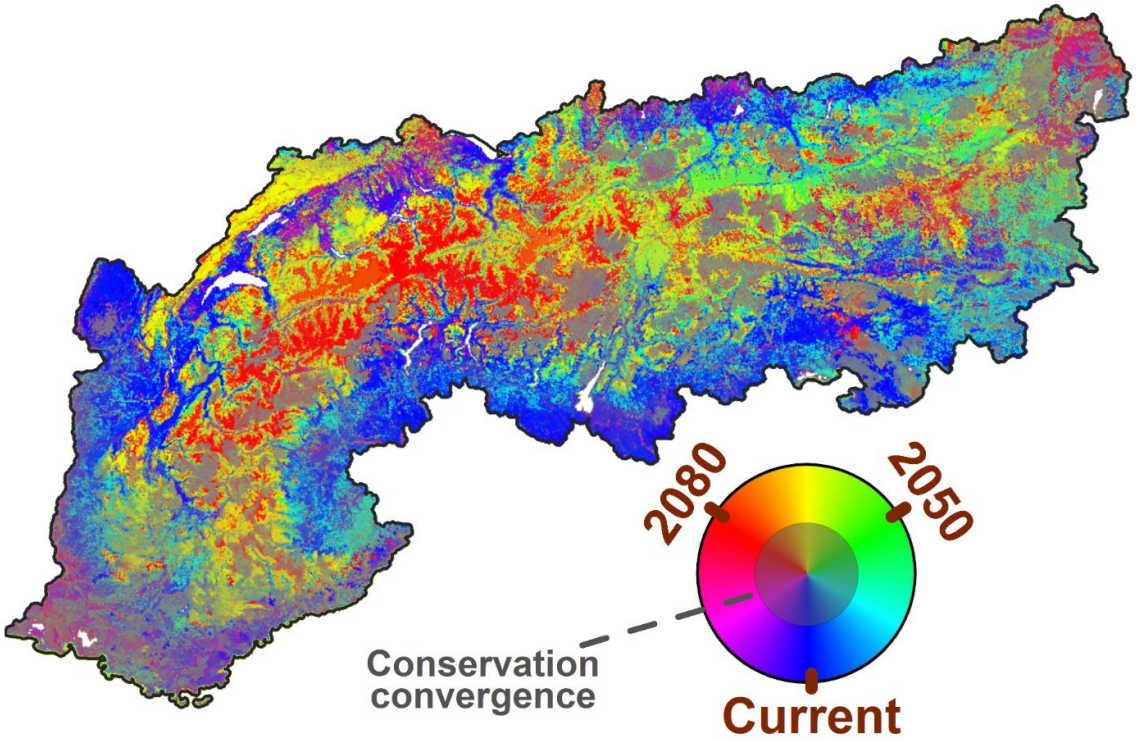

Figure S6. Current and future local conservation needs in the European Alps for SSP585 and realistic plant dispersal, under ZONATION simulations of reserve network expansion.

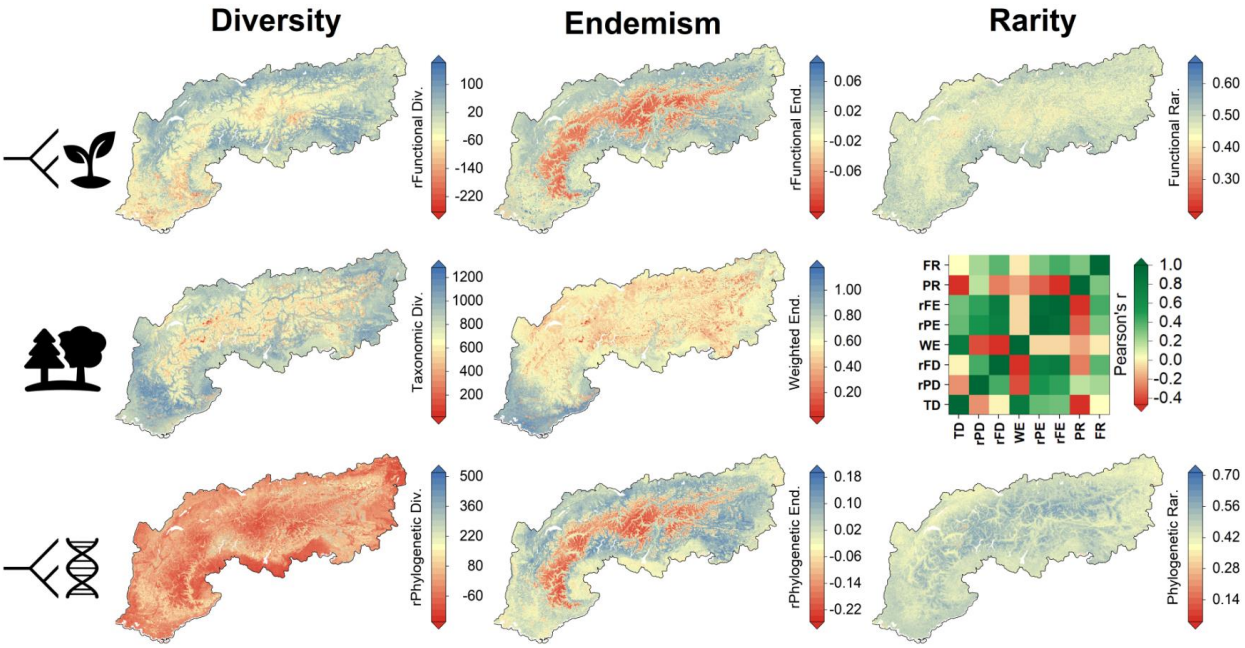

Figure S7. Current distribution of multifaceted diversity and uniqueness in the European Alps. First, second and third row depict the functional, taxonomic and phylogenetic dimension respectively. Middle right raster plot shows Pearson's correlation relationships between all maps. TD, rPD and rFD: taxonomic, relative phylogenetic and functional diversity; WE, rPE and rFE: weighted taxonomic, relative phylogenetic and functional endemism respectively; PR and FR: phylogenetic and functional rarity.

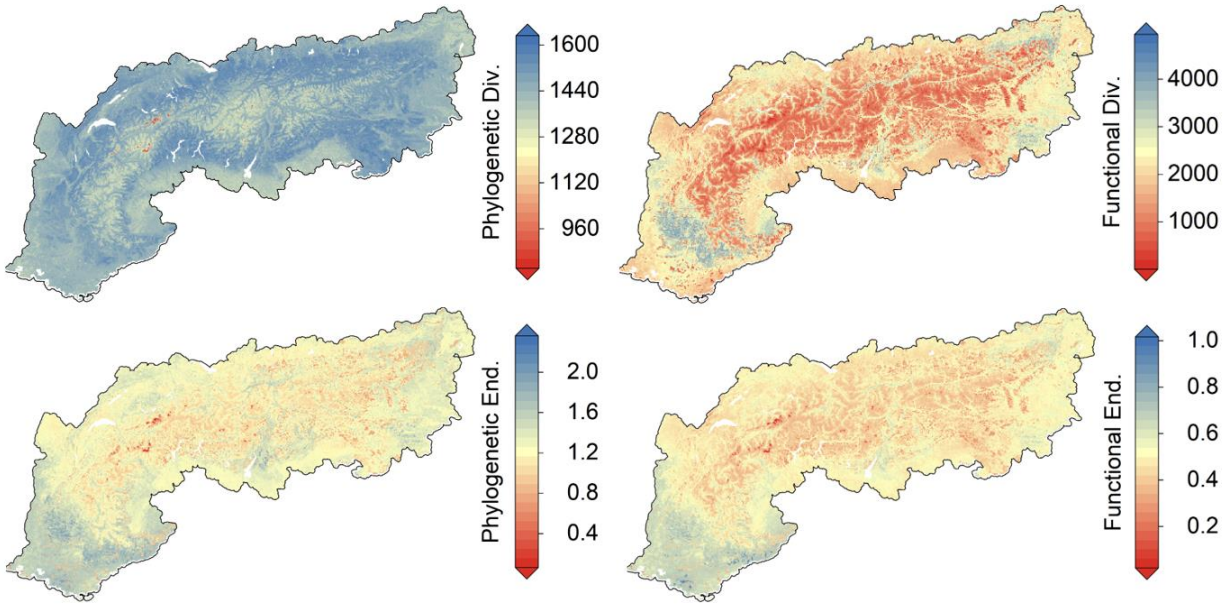

Figure S8. Distribution of current phylogenetic, functional diversity and endemism in the European Alps. Here are depicted the absolute version of the four diversity features.

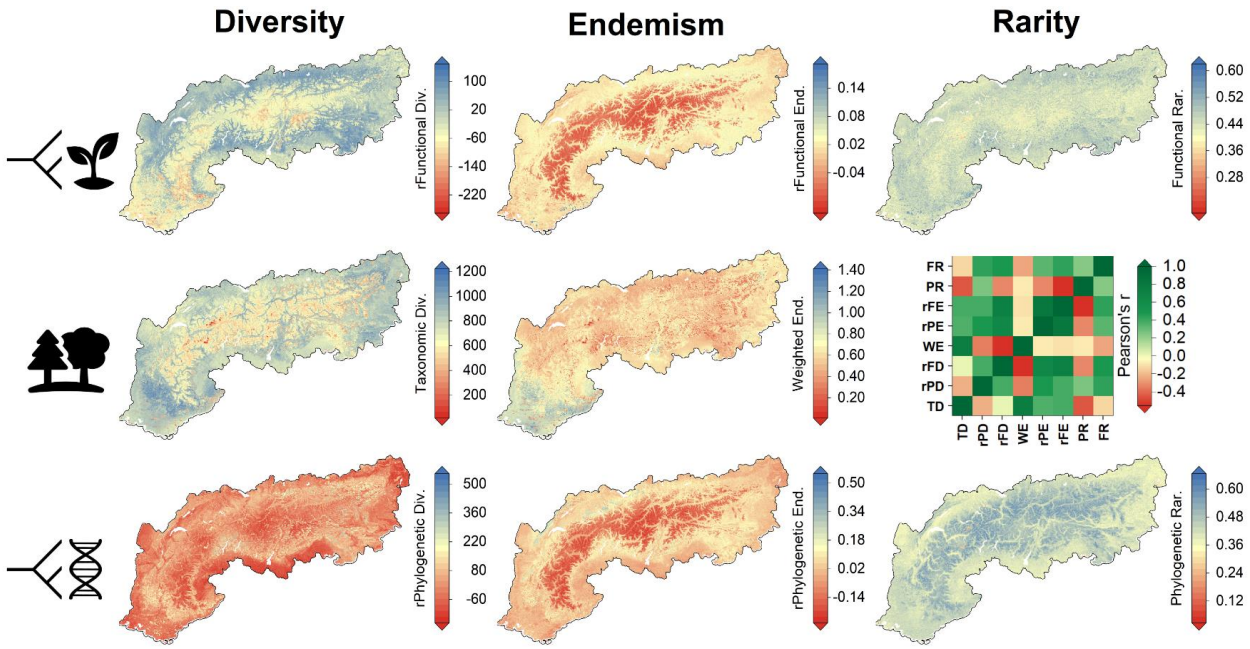

Figure S9. Distribution of multifaceted diversity and uniqueness in the European Alps by 2050 for SSP245 and realistic plant dispersal.

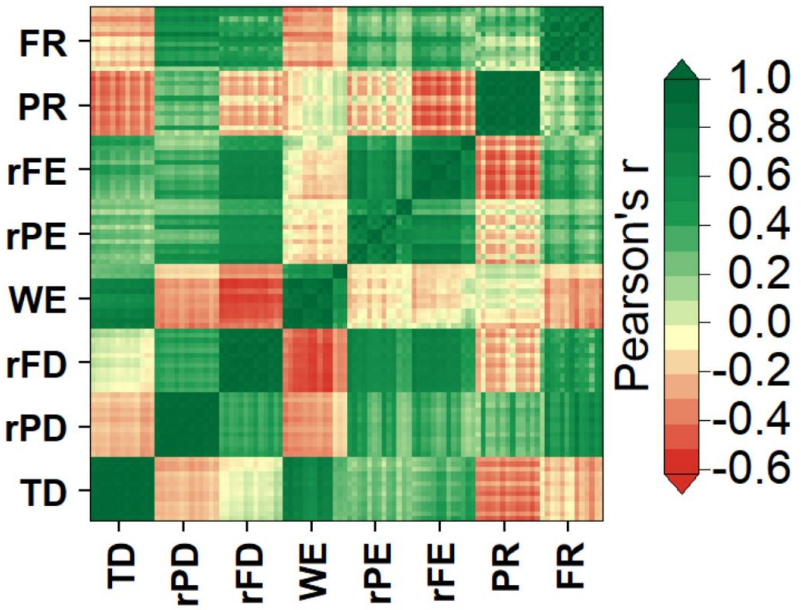

Figure S10. Pearson's correlation relationships between all multifaceted diversity and uniqueness maps generated for the study. Correlations are assessed for a total of 104 diversity and uniqueness maps. Each x and y axis label includes in total 13 maps; i.e. per current and 12 future timeline/SSP/dispersal scenarios. Overall, general patterns follow the correlation relationships found above. TD, rPD and rFD: taxonomic, relative phylogenetic and functional diversity; WE, rPE and rFE: weighted taxonomic, relative phylogenetic and functional endemism respectively; PR and FR: phylogenetic and functional rarity.

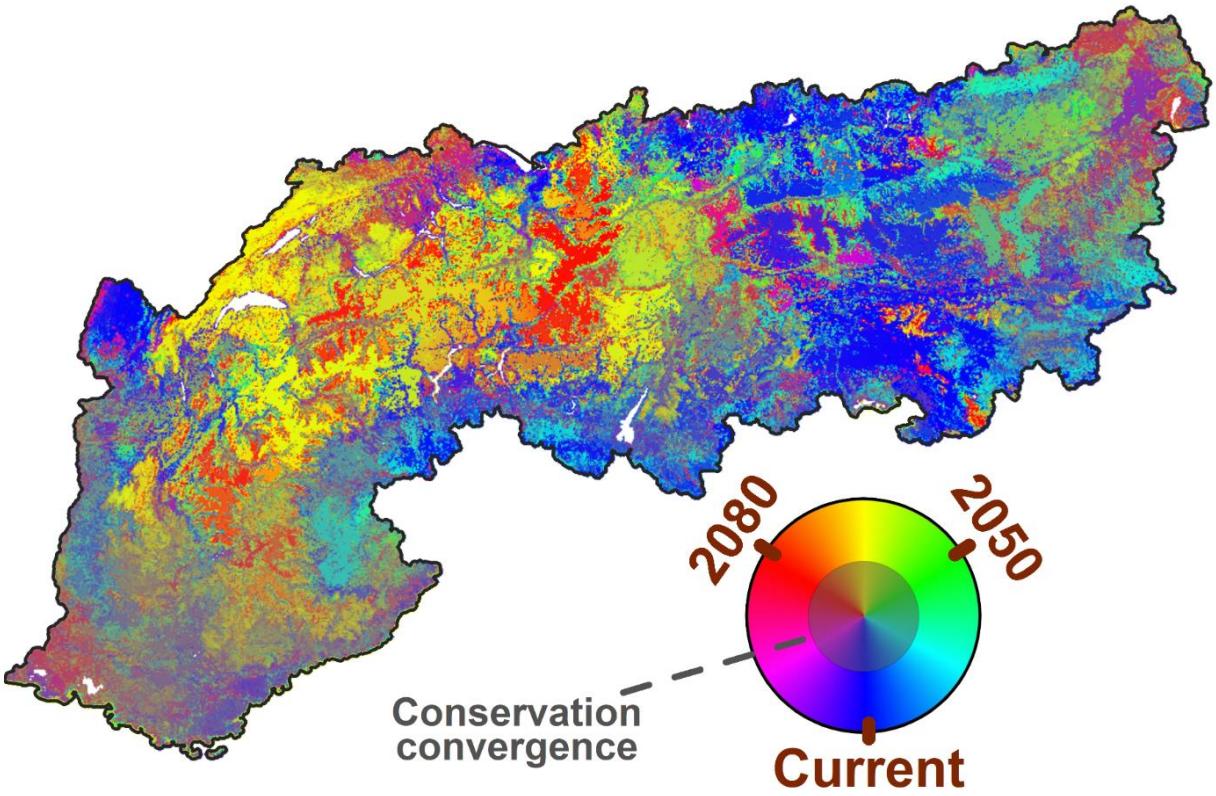

Figure S11a. Current and future local conservation needs in the European Alps for SSP245 and realistic plant dispersal, under ZONATION simulations of optimal reserve network.

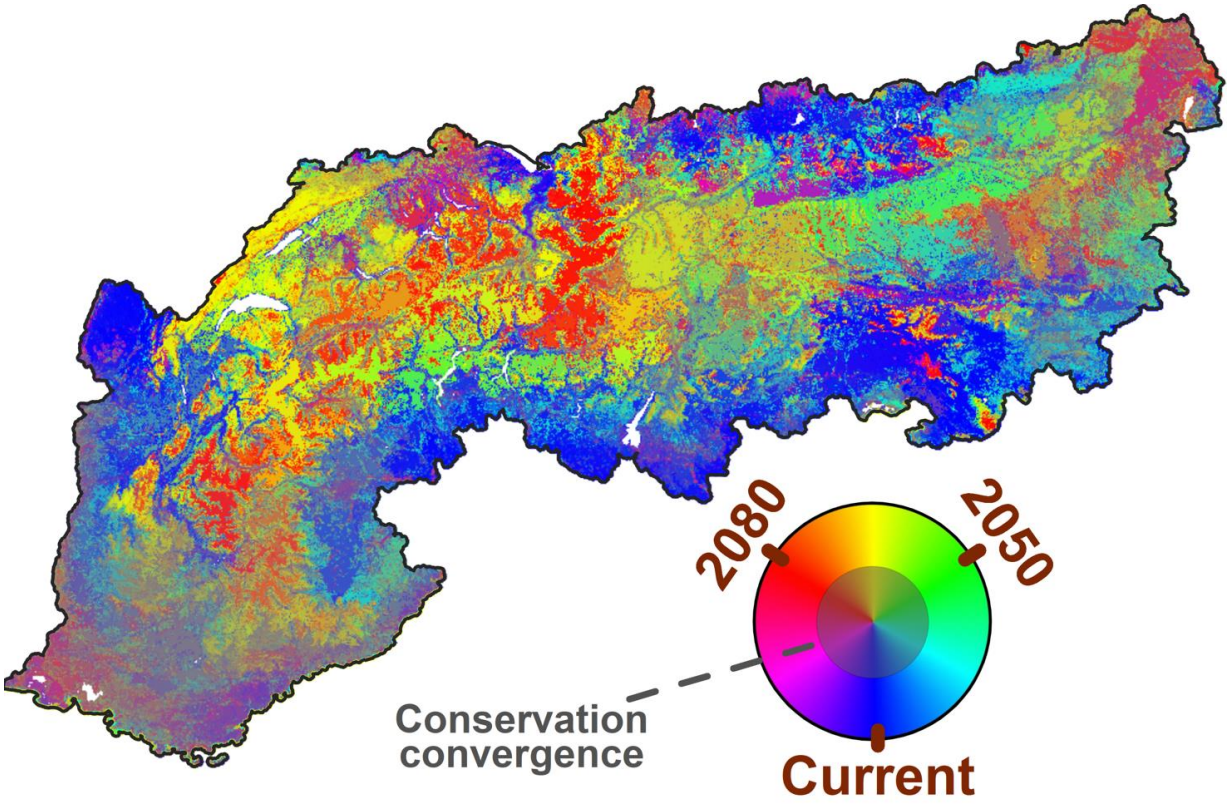

Figure S11b. Current and future local conservation needs in the European Alps for SSP585 and realistic plant dispersal, under ZONATION simulations of optimal reserve network.

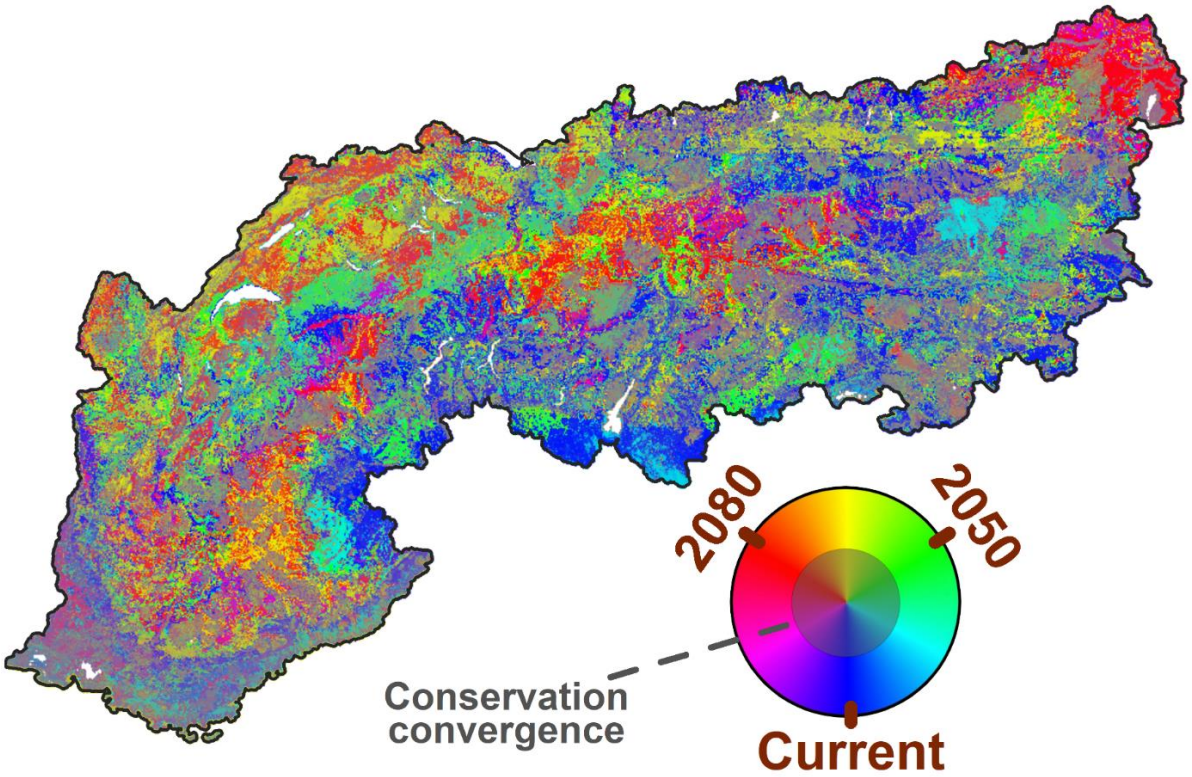

Figure S11c. Current and future regional conservation needs in the European Alps for SSP245 and realistic plant dispersal, under ZONATION simulations of reserve network expansion.

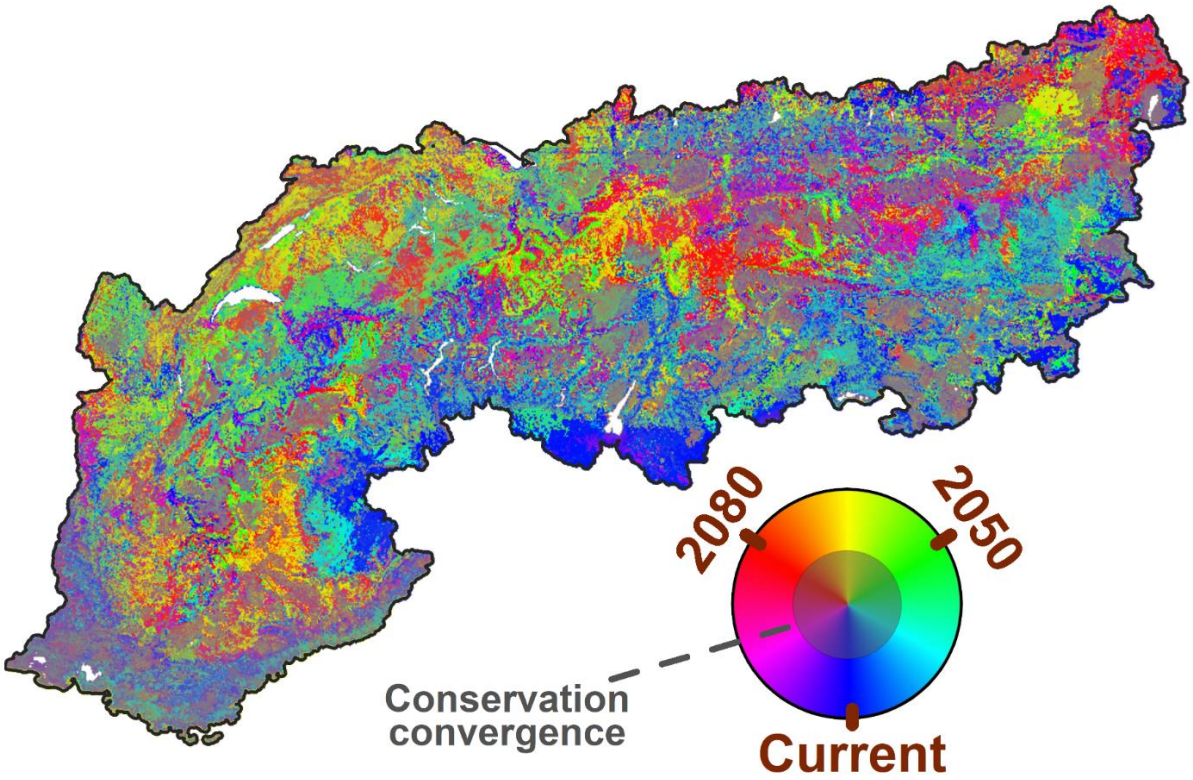

Figure S11d. Current and future regional conservation needs in the European Alps for SSP585 and realistic plant dispersal, under ZONATION simulations of reserve network expansion.

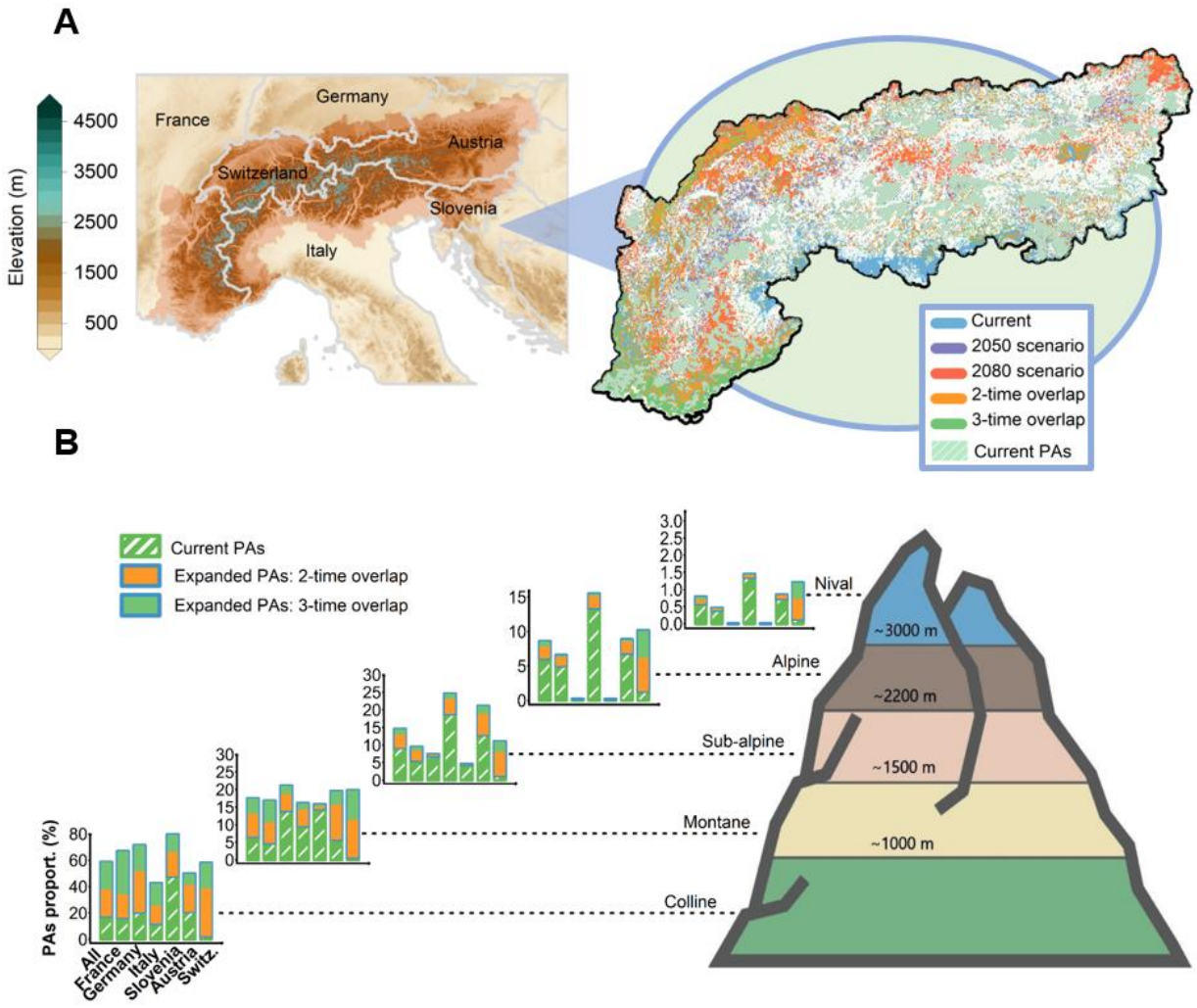

Figure S12. Distribution of the current protected areas (PAs) network of the European Alps and it future (top 20%) regional expansion for SSP585 and realistic plant dispersal.

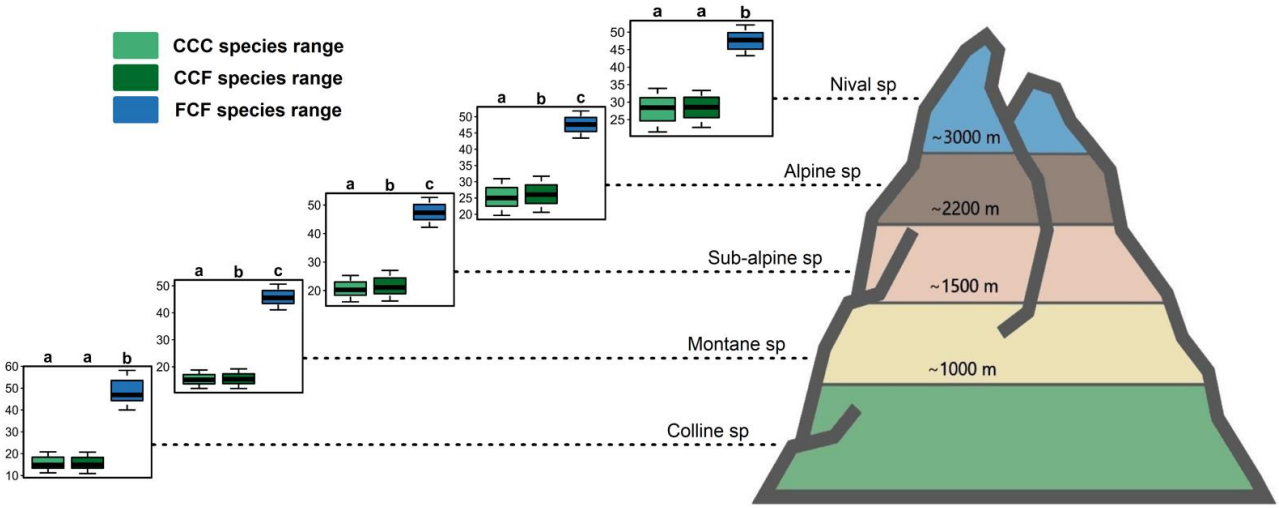

Figure S13. Summary of species range protection for current (green) and expanded PAs (blue) in 2050 under SSP245 and realistic plant dispersal. Expanded PAs represents the top 20% regional expansion of the reserve network of the European Alps. CCC: current conservation of current species range, CCF: current conservation of future species range, FCF: future conservation of future species range. *Friedman tests* were applied here for each panel to compare the median values of the three boxplots. All pairwise comparisons were run with post-hoc *Nemenyi tests* and displayed following a letter-based representation (*p-value* > 0.05).

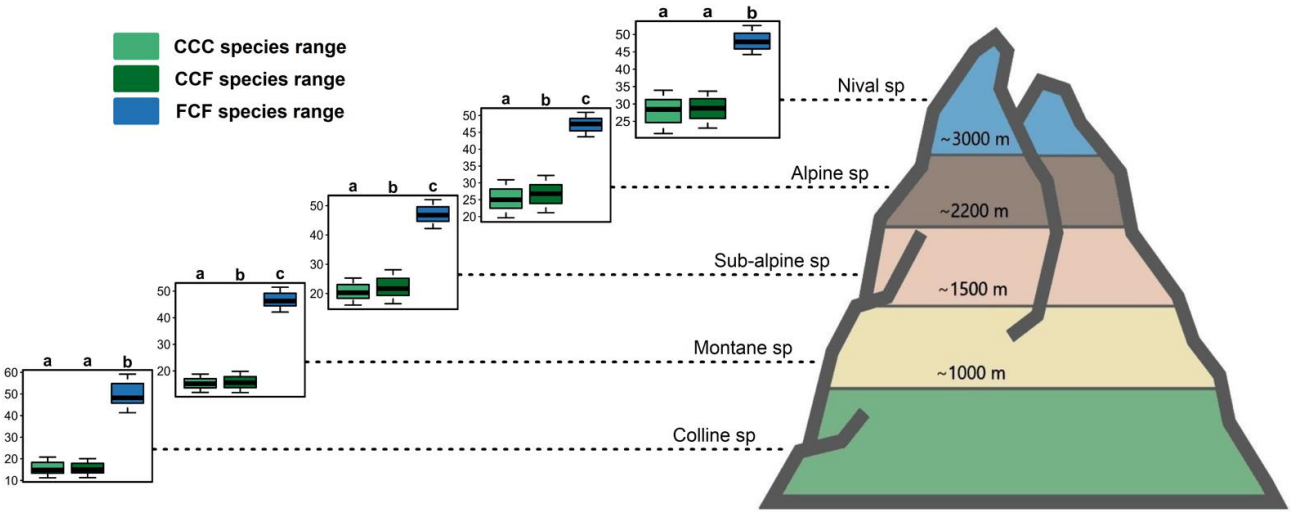

Figure S14. Summary of species range protection for current (green) and expanded PAs (blue) in 2050 under SSP585 and realistic plant dispersal.

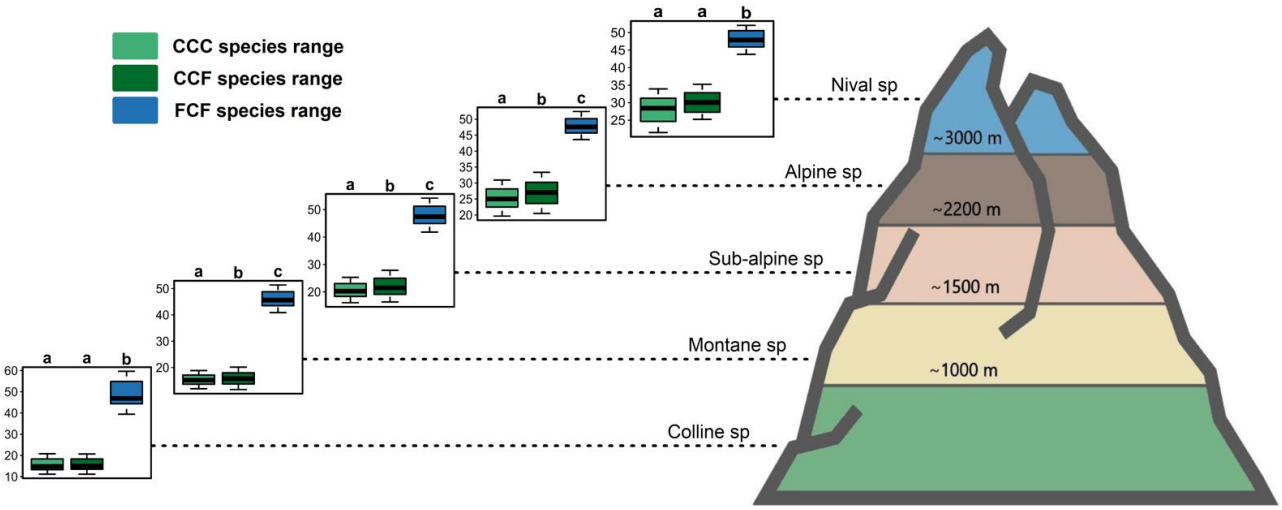

Figure S15. Summary of species range protection for current (green) and expanded PAs (blue) in 2080 under SSP245 and realistic plant dispersal.

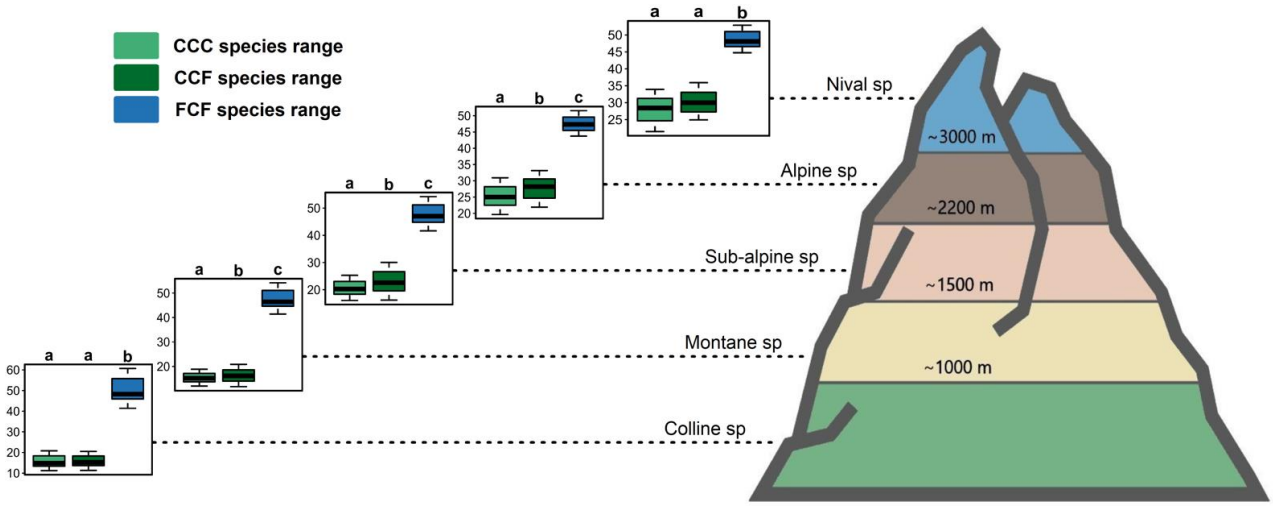

Figure S16. Summary of species range protection for current (green) and expanded PAs (blue) in 2080 under SSP585 and realistic plant dispersal.

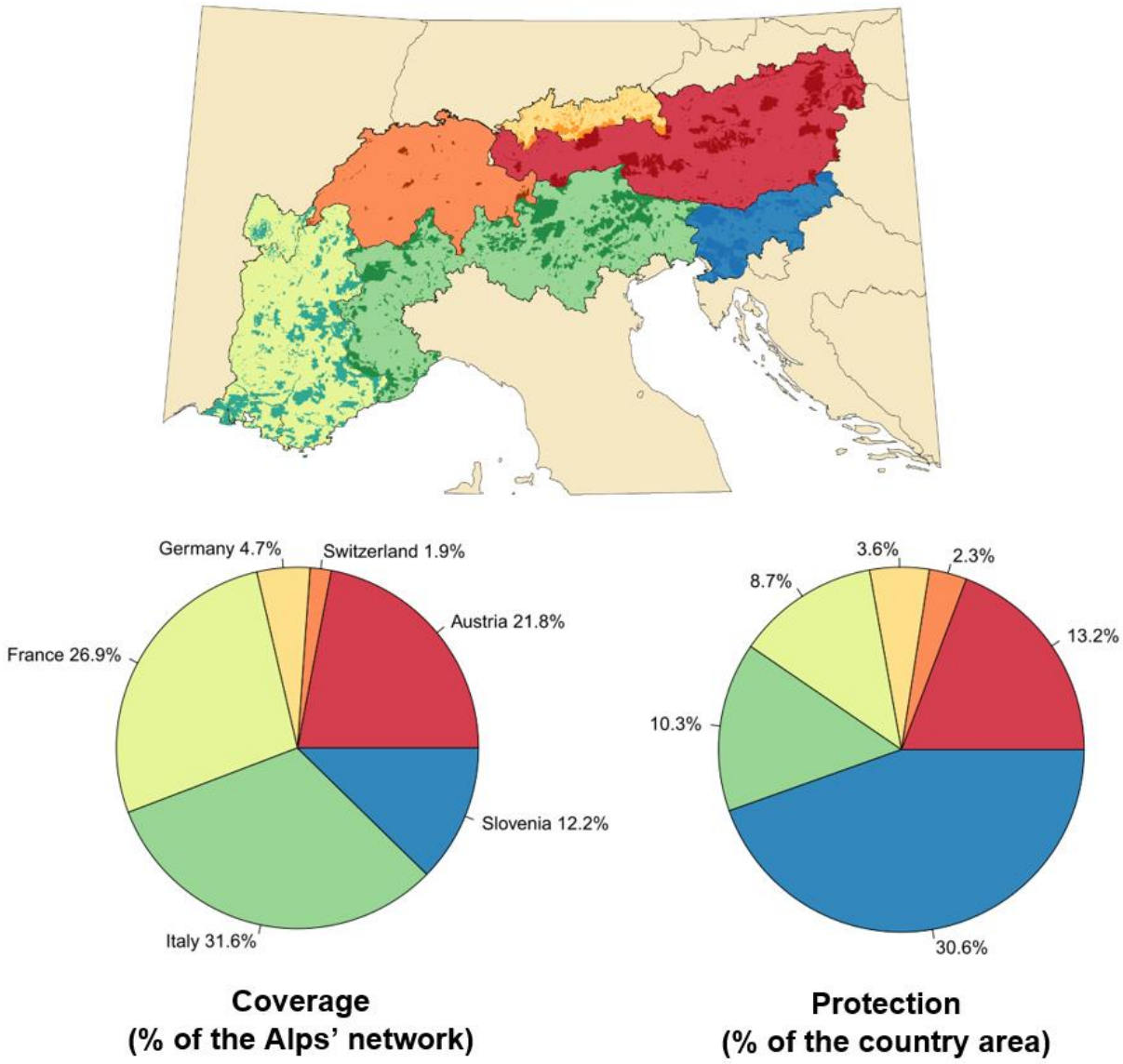

Figure S17. Spatial coverage and protection statistics of the European Alps' reserve network (IUCN categories I-II and Natura 2000) for the six main countries member of the Alpine Convention. Left panel depicts the area of the reserve network (in %) covered by each country. Right panel depicts the percentage of area protection relative to the countries' area.

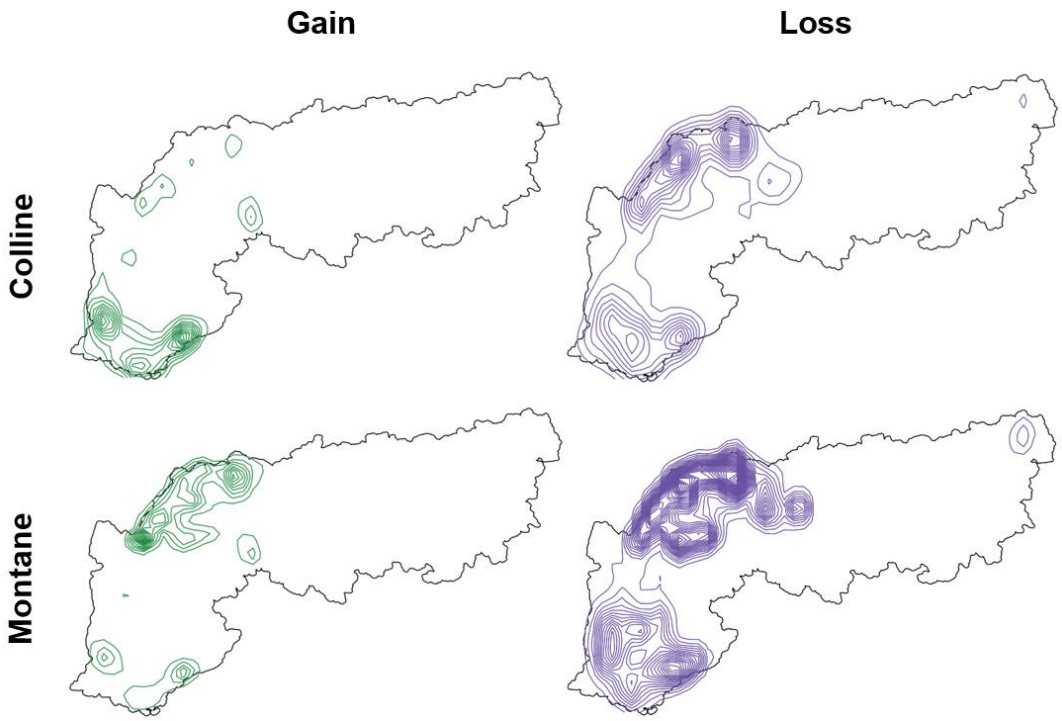

Figure S18. Observation density of colline (upper) and montane species (lower) undergoing high future range gain (left) and loss (right) by 2050 for SSP245 and realistic plant dispersal. High gains and losses are defined as > 75th quantile of all species' range gains and losses, respectively. Green and purple upper contour lines summarize the observation density of 65 (n = 82,133 records) and 56 species (n = 29,762 records) respectively. Green and purple lower contour lines summarize the density of 61 (n = 144,776 records) and 94 species (n = 72,642 records) respectively.

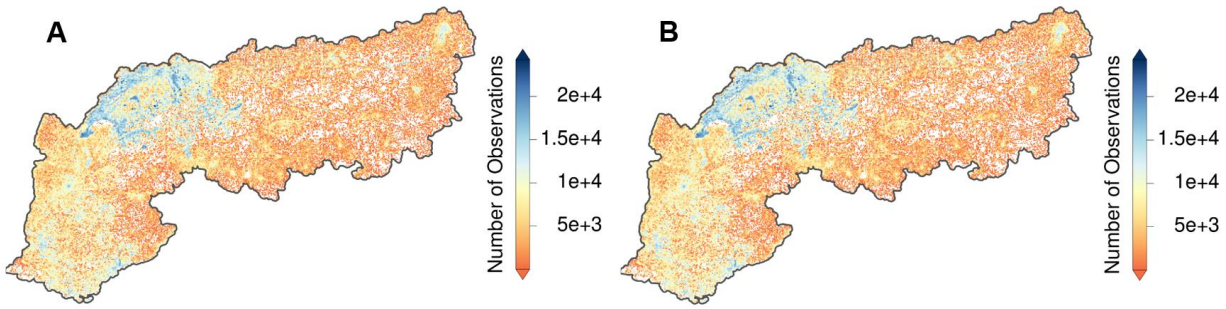

Figure S19. Distribution density of our original (a) and refined species observational dataset (b) across the extended European Alps. (**A**) shows the target group observation density of the original observational dataset (i.e. 6'655'163 observations accurate to 11.1 meters for 4’250 species). (**B**) shows the observation density of our refined observational dataset (6'603'305 unique observations for 3’167 species), i.e. the whole species observations used for model calibration. Distribution of density was aggregated at 2 km resolution for better visual representation and log transformed.

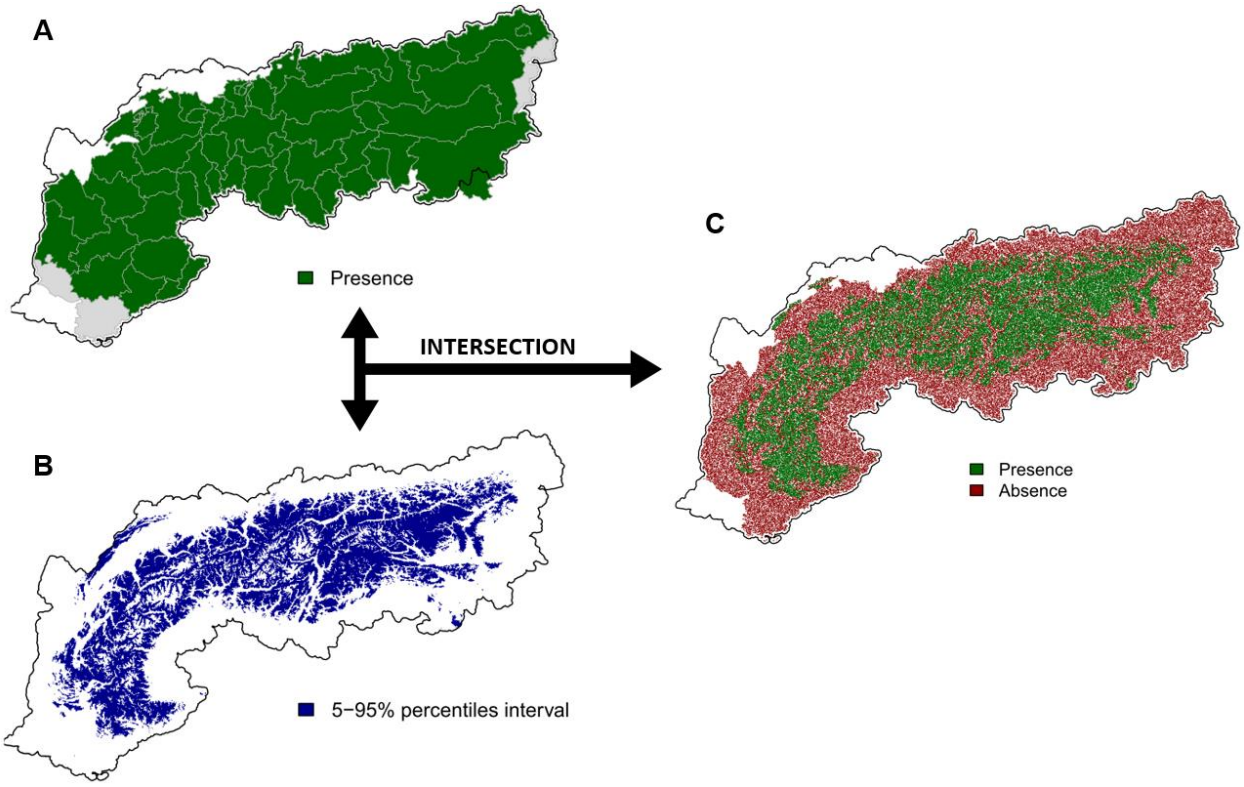

Figure S20. Methodological framework used to generate the FA independent test dataset at 100 m resolution. Here is presented an example for *Soldanella alpina*. The initial FA raw distribution of *Soldanella alpina* (**A**) is summarized within 54 expert-based native political units (green is regional presence) [1] and was intersected with the 5-95% percentiles elevation interval of *Soldanella alpina* (**B**). This interval here corresponds of an elevational range of ~1'016 - 2'453 m. It was calculated by extracting values of the DEM over Europe (EU-DEM; https://www.eea.europa.eu/data-and-maps/data/eu-dem), aggregated to 100 x 100 m resolution, with the 8'841 species observations. Final output was a refined independent binary distribution of *Soldanella alpina* from which we inferred 100 m presences and absences, sampled n times afterwards for independent evaluation (**C**). Here, as an example, 100'000 presences and absences were plotted respectively.

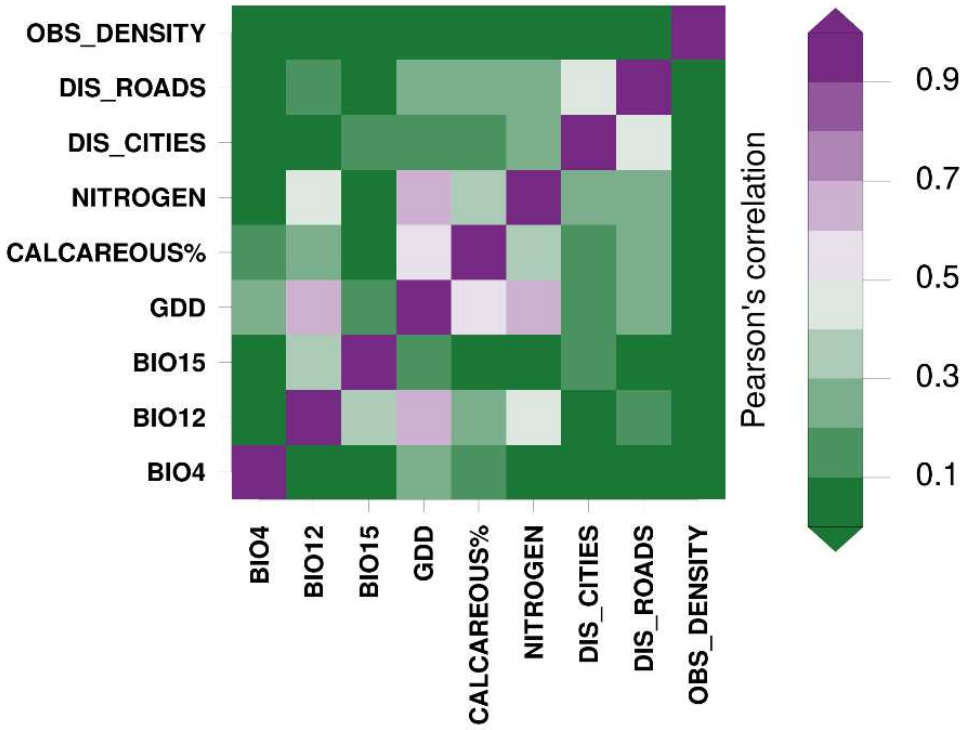

Figure S21. Pearson correlation tests between every environmental predictor (except categorical land cover) and bias covariate considered in our models. Climate included growing degree days (GDD), annual precipitation (BIO12), temperature (BIO4) and precipitation seasonality (BIO15). Soil included soil nitrogen (NITROGEN) and substrate composition (CALCAREOUS%). The bias covariates included observation density (OBS_DENSITY), distance to roads (DIS_ROADS) and cities (DIS_CITIES).

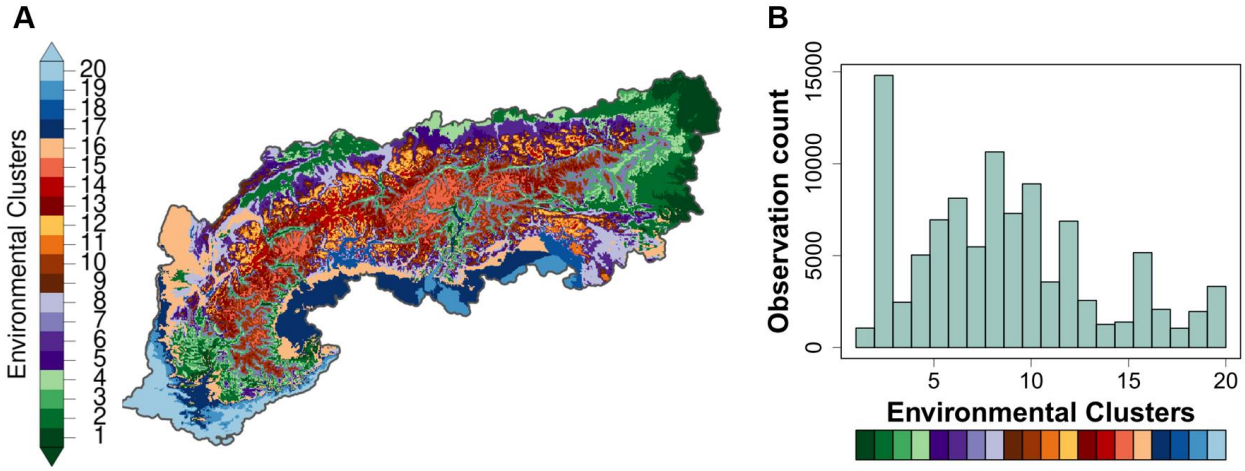

Figure S22. Environmental cluster distribution and frequency in observations across the study region. (**A**) describes the distribution of the 20 environmental clusters over the study area obtained with the R function *wsl.ebc* [2]. Those were obtained at 100 m resolution based on our four climate and two soil variables. (**B**) summarizes the species observation frequencies per environmental cluster regarding the refined observational dataset. Here, 100'000 species observations were sampled randomly without replacements over the cluster map. We see that the sampling design of our refined observational dataset is environmentally biased towards cluster 2 and clusters 5 to 12, i.e. the environmental space of Switzerland (~50% of the refined observational dataset).

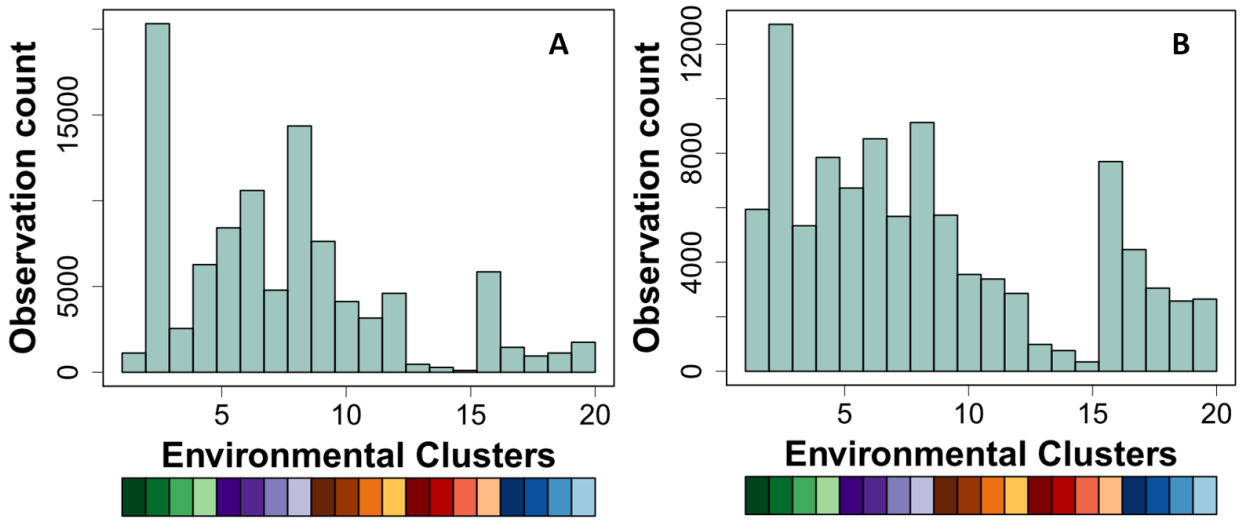

Figure S23. Species observation frequencies per environmental cluster before (**A**) and after EBC (**B**) for the 1248 corrected species across the study region. Here, 100'000 non-corrected (**A**) and corrected species observations (**B**) were sampled randomly without replacements over the cluster map. We see that the sampling design in (**A**) is, as the refined observational dataset, environmentally biased towards cluster 2 and clusters 5 to 12, whereas in (**B**), observations frequencies were balanced across environmental clusters based on their respective log(area).

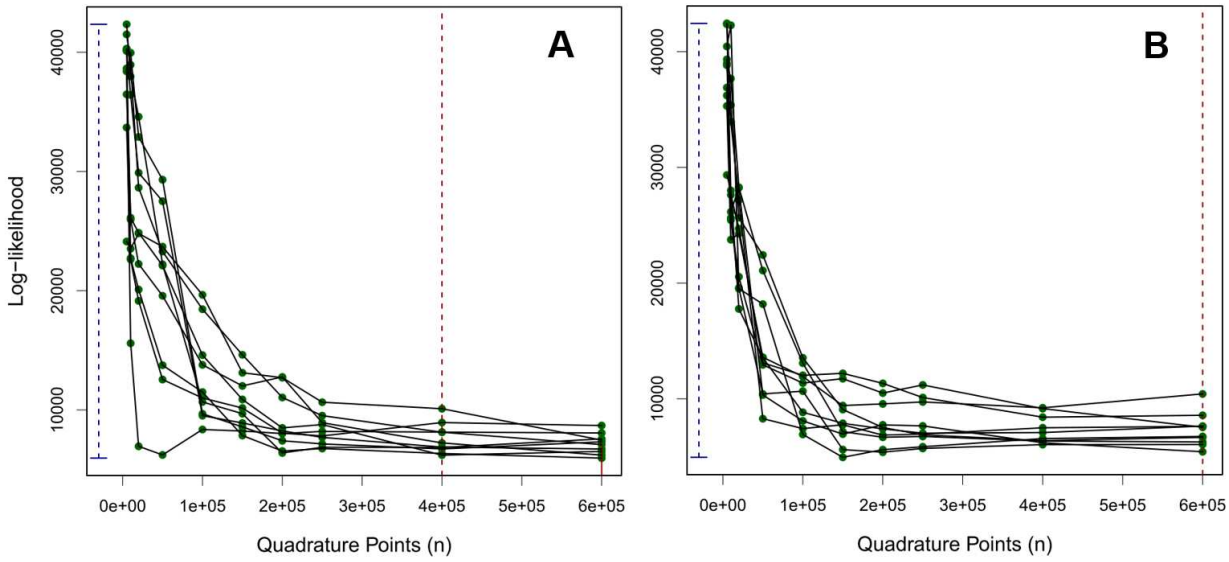

Figure S24. An example of PPM log-likelihood convergence for *Soldanella alpina*. Here are shown the PPM convergence tests for models including as land cover the ECOCHANGE (**A**) and HERCULES categories (**B**). To obtain the adequate number of quadrature points, convergence tests were applied before model calibration. For this, 10 preliminary repeated series of DWPR were run, each one gradually increasing the number of randomly sampled quadrature points (i.e. 5000, 10'000, 20'000, 50'000, 100'000, 150'000, 200'000, 250'000, 400'000, 600'000). Below solid red line indicates number of quadrature points chosen by the test (e.g. in a, n = 600'000); i.e. position on the x axis where standard deviation of the log-likelihood values < 10% of the standard deviation found in x = 5000. Dotted blue line indicates range of log-likelihood values for x = 5000. Dotted red line indicates the last position on the x axis where standard deviation of the log-likelihood values > 10% of that of found in x = 5000. Note that if no solid red line appeared (e.g. in **B**), a high number of quadrature points (n = 1'000'000) was chosen by default following [2].

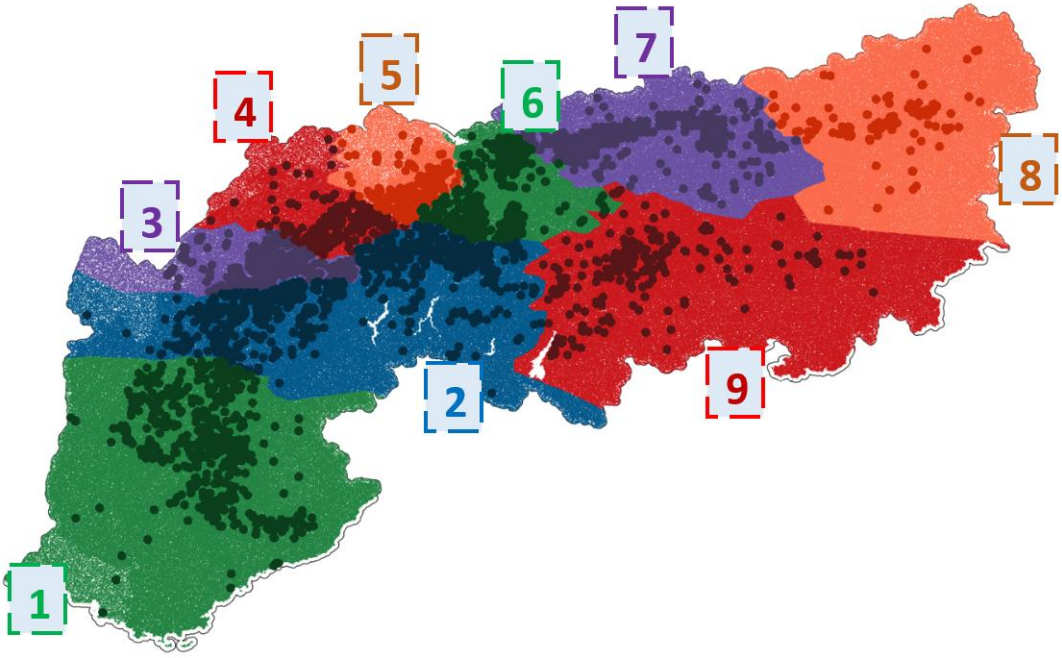

Figure S25. Example of spatial block split sampling for *Soldanella alpina*. Following [3], its 8'755 observations (here highlighted in darker colors) were evenly partitioned into 9 blocks of 5 folds spatially stratified (~2 blocks per fold; numbers are indicated) using species observation coordinates, partitioning around medoids (PAM) clustering and the R package *cluster* (function *pam*) [4–6]. This allowed the number of observations to be spatially and numerically balanced within each independent fold. It is important to note that, even though the number of blocks was set to 10, this number may slightly vary per species conditional on the best balancing strategy of the PAM algorithm. Fold 1 (purple), 2 (red), 3 (orange), 4 (blue) and 5 (green) here contains 1'755, 1'538, 1'536, 1'976 and 1'950 species observations respectively. Sampled quadrature points and Flora Alpina presences/absences (here highlighted in lighter colors) were assigned to each independent block using k-nearest neighbor classification and the R package *class* (function *knn*) [7,8]. For every species and models (PPM), the same number of Flora Alpina presences/absences as quadrature points were sampled, to ensure balanced repartitioning among folds.

A

```
    Test of normality and Homoscedasticity:
  ----------------------------------------

Hawkins Test:

    P-value for the Hawkins test of normality and homoscedasticity:  0

    Either the test of multivariate normality or homoscedasticity (or both) is rejected.
    Provided that normality can be assumed, the hypothesis of MCAR is
    rejected at 0.05 significance level.

Non-Parametric Test:

    P-value for the non-parametric test of homoscedasticity:  5.812039e-13

    Hypothesis of MCAR is rejected at  0.05 significance level.
    The multivariate normality test is inconclusive.
```

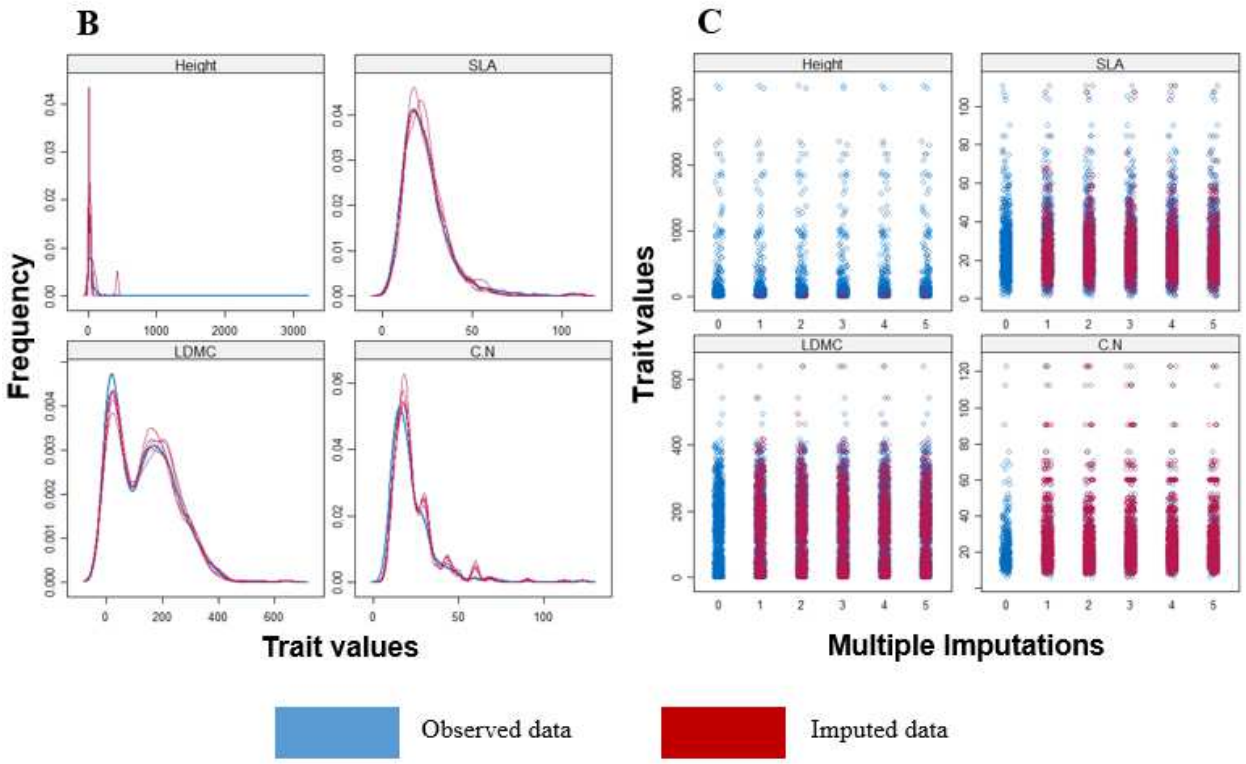

Figure S26. Preliminary MCAR (**A**) and multiple-imputation tests (**B**, **C**). MCAR test was run with the *TestMCARNormality* function (*MissMech* R package) [9]. Multiple imputation tests were run 5 times with the *mice* function (*mice* R package) [10] using the random forest method (following *68*). (**A**) shows R output of the *TestMCARNormality* function. MCAR-test is negative with *P-value* > 0.05. Missing trait values are therefore not missing completely at random. (**B**) shows the distribution frequency plot of four trait values (Height, SLA - specific leaf area, LDMC - leaf dry matter content and C:N - carbon to nitrogen ratio). Blue line represents the distribution of observed trait values whereas the five red lines represent the distribution of imputed values from each five multiple-imputations. (**C**) follows same color legend and shows same distribution as individual points (or Stripplot). The very similar distributions between observed and imputed data found here gives strong evidences that missing trait values follow a MAR assumption [10].

Table S1. Description of extinct species for current and future scenarios. Information on their respective elevation class, soil substrate and vegetation type is also given.

SSP	Timeline	Dispersal	Extinct Species	Elevation Class	Substrate	Type
	Current					
SSP245	2050	Realistic				
SSP245	2050	Unlimited				
SSP245	2050	No				
SSP245	2080	Realistic	*Antirrhinum latifolium*	Montane	Calcareous	Herbaceous
SSP245	2080	Unlimited	*Antirrhinum latifolium*	Montane	Calcareous	Herbaceous
SSP245	2080	No	*Antirrhinum latifolium*	Montane	Calcareous	Herbaceous
SSP585	2050	Realistic	*Iberis saxatilis*	Sub-alpine	Calcareous	Herbaceous
SSP585	2050	Unlimited	*Iberis saxatilis*	Sub-alpine	Calcareous	Herbaceous
SSP585	2050	No	*Iberis saxatilis*	Sub-alpine	Calcareous	Herbaceous
SSP585	2050	Realistic	*Antirrhinum latifolium, Iberis saxatilis*			
SSP585	2050	Unlimited	*Antirrhinum latifolium, Iberis saxatilis*			
SSP585	2050	No	*Antirrhinum latifolium, Iberis saxatilis*			

Table S2. Complete list of sources of species observations.

Sources	Observations Count	Contribution
AAAAA	18903	0,245316177942023
ACBOG	2	2,595526402603e-05
AIPHY	686	0,0089026555609283
ALOBO	3	3,8932896039045e-05
ANSES	43	0,000558038176559645
ASTER	1303	0,0169098545129586
ATFHA	362	0,00469790278871143
AVENI	57	0,000739725024741855
BDMZ7	96186	1,24826651280386
BDONF	7393	0,09594363347222
BIOTO	42	0,00054506054454663
BMDZ9	34265	0,444678560925959
CAT07	7488	0,0971765085134564
CBNA	206809	2,68389109897962
CBNME	158	0,00205046585805637
CBNMED	431630	5,60153530577767
CENP	118	0,00153136057753577
Cerabo	374	0,00485363437286761
CHLAU	1703	0,0221009073181646
CINCL	4	5,191052805206e-05
DISEQUALP	30289	0,393079496042212
ECODI	9063	0,117616278933955
ECOME	281	0,00364671459565722
ECOSP	1165	0,0151189412951625
EHB	11772	0,152772684057213
ENGRE	1104	0,0143273057423686
ESITP	34	0,00044123948844251
EVINE	128	0,00166113689766592
FLAVI	468	0,00607353178209102
FRAPN	14	0,00018168684818221
GBIF	2242347	29,1003542114882
HERZO	2	2,595526402603e-05
INFLO	1692	0,0219581533660214
InfoFlora	4027105	52,2622867677728
JORDE	86	0,00111607635311929
KarstData	26900	0,349098301150104
LAVAN	62	0,00080461318480693
LEPJH	102	0,00132371846532753
LOPAR	6	7,786579207809e-05
MNHN	51	0,000661859232663765
NAENV	28	0,00036337369636442
NEOT	60	0,000778657920780901

ONF	4738	0,0614880204776651
PNE	14713	0,19093989980749
PNM	335	0,00434750672436003
PNRLU	647	0,00839652791242071
PNRMB	537	0,00696898839098906
PNRQ	371	0,00481470147682857
PNV	238	0,00308867641909757
RECAL	10	0,00012977632013015
RESBO	2847	0,0369473183410537
RESCB	654	0,00848737133651182
RNLAV	171	0,00221917507422557
RNPLA	1	1,2977632013015e-05
SAGEE	32	0,00041528422441648
SBCOU	21	0,000272530272273315
SBDRO	37	0,000480172384481555
SBF	242	0,00314058694714963
SBNF	193	0,0025046829785119
SDETB	239	0,00310165405111059
SERAN	62	0,00080461318480693
SHNPM	12	0,00015573158415618
SIGDA	60	0,000778657920780901
SLL	1	1,2977632013015e-05
TUXEN	10	0,00012977632013015
TWW	419115	5,43912024113478
UAMSJ	3057	0,0396726210637869
UCLBL	12	0,00015573158415618
UCOMA	104	0,00134967372935356
UNBES	2336	0,0303157483824031
UNDST	126	0,00163518163363989
UNJOF	14443	0,187435939163976
UNPRO	1479	0,0191939177472492
UPAXI	3827	0,0496653977138084
WILLNER	52125	0,676459068678407
X	8	0,00010382105610412
ZER	22475	0,291672279492512

Table S3. Statistics of the original (4’250 species) and refined observational dataset (3’167 species).

	Original dataset	*Refined dataset*
Minimum	1	30
1st Quantile	41	199
Median	305	607
Mean	1566	2085
3rd Quantile	1368	2123
Maximum	42948	42948

Table S4. List of predictors used in the EIV mapping. The description and the source of each predictor is provided.

Layer name	Abbreviation	Description	Sources of the layers
DEM_laea_100m	DEM	Digital elevation model	https://www.eea.europa.eu/data-and-maps/data/copernicus-land-monitoring-service-eu-dem
DEM_aspect_laea_100m	Aspect	Aspect	This manuscript, using function *terrain* and R 3.6
DEM_TPI_laea_100m	TPI	Topographic position index	This manuscript, using function *terrain* and R 3.6
DEM_TRI_laea_100m	TRI	Topographic roughness index	This manuscript, using function *terrain* and R 3.6
DEM_TWI_SAGA_laea_100m	TWI	Topographic wetness index	This manuscript, using SAGA-GIS 7.2.0
OPENSTREET_h20_dis_laea_100m	H20	Distance to water	https://www.openstreetmap.org/#map=11/47.0056/7.9740 - Layer calculated with R 3.6, python 3.6 and GDAL
GLIM_bedrock_types_laea_100m	Geology	Soil geology reclassified in three groups (gradient of CaCO3)	[12] based on [13]

Table S5. Spearman rank correlations between observed and predicted EIVs based on repeated split-sampling (Split) and five-fold block cross-validation (CV) tests in the European Alps. EIV-R = soil pH. EIV-N = soil nitrogen, EIV-F = soil moisture.

EIV	Split		CV	
	r		r	
	Mean	SD	Mean	SD
EIV-R	0.843	0.001	0.835	0.029
EIV-N	0.867	0.001	0.852	0.032
EIV-G	0.825	0.002	0.819	0.043
EIV-F	0.860	0.003	0.853	0.027

Table S6. Reclassified VOLANTES-HERCULES land cover from 16 to 10 classes.

HERCULES land cover	***Reclassified land cover***
Built-up area	Built-up area
Arable land (non-irrigated)	Arable land (non-irrigated)
Pasture	Pasture
Semi-Natural vegetation	Semi-Natural vegetation
Irrigated arable land	Irrigated arable land
Permanent crops	Permanent crops
Forest	Forest
Sparsely vegetated areas	Others
Beaches, dunes and sands	Others
Inland wetlands	Others
Glaciers and snow	Others
Heather and moorlands	Others
Salines	Removed
Water and coastal flats	Removed

Table S7. Complete list of sources of trait data

SOURCES	NUMBER OF SAMPLES	CONTRIBUTION (%)
ARVES 2012	7635	4.48906397
BISON	1300	0.76434619
BRZEZIECKI & KIENAST, 1994	26	0.015286924
CBNA	9365	5.506232361
CHOLER	196	0.115239887
COLACE	779	0.458019755
CORNELISSEN, 1999	48	0.028222013
CORNELISSEN, UNPUBLISHED DATA	115	0.06761524
DISEQUALP	5349	3.144990593
ECOCHANGE	498	0.292803387
EQUIPE TDE	11825	6.952610536
FIFTH	28765	16.91262935
FLORA ALPINA	248	0.145813735
FLORA OF ESTONIAN NSV	1166	0.685559737
HYDROTRDB	4735	2.783984008
INTRABIODIV	2522	1.482831609
KEW SEED INFORMATION DATABASE	193	0.113476011
LEDA	11001	6.468132643
LESTRUECSPE	12381	7.279515522
MOUVE	668	0.39275635
MSS	1351	0.794332079
NIINEMETS AND KULL, 2003	60	0.035277516
ODYSSEE	5882	3.458372531
ODYSSEE	155	0.091133584
OLO	700	0.411571025
ORIGINALPS	31650	18.60888993
SCHWEINGRUBER	3199	1.880879586
STACE, 1991	82	0.048212606
TTT_ALPS	3795	2.231302916
TTT_NON_ALPS	23684	13.92521167
VAN DER MEIJDEN ET AL., 1990	74	0.043508937
VITTOZ&ENGLER	508	0.298682973
WILLNER	125	0.073494826

Table S8. Chosen Zonation parameters

Zonation setting file (.dat)	Zonation feature list file (.ssp)
removal rule = 1 (CAZ) or 2 (ABF)	*weight* = sp PU[1] + sp FU[2]
warp factor = 100 [14]	*alpha* = 1 (default)
use mask = 0 (selection) or 1 (expansion)	*bqp* = 1 (default)
mask file = I-II-2000_IUCN.tif	*bqp_p* = 1 (default)
	cellrem = 0.25 [14]

[1] Phylogenetic Uniqueness

[2] Functional Uniqueness

Parameters in blue were chosen by default, i.e. connectivity settings off.

Table S9. Description of the 26 priority maps generated for each CAZ and ABF algorithm

	Year	Emissions	Dispersal	IUCN I-II reserves + Natura 2000
1	Current			Yes
2	Current			No
3	2050	SSP245	no dispersal	Yes
4	2050	SSP245	no dispersal	No
5	2050	SSP245	unlimited dispersal	Yes
6	2050	SSP245	unlimited dispersal	No
7	2050	SSP245	realistic dispersal	Yes
8	2050	SSP245	realistic dispersal	No
9	2050	SSP585	no dispersal	Yes
10	2050	SSP585	no dispersal	No
11	2050	SSP585	unlimited dispersal	Yes
12	2050	SSP585	unlimited dispersal	No
13	2050	SSP585	realistic dispersal	Yes
14	2050	SSP585	realistic dispersal	No
15	2080	SSP245	no dispersal	Yes
16	2080	SSP245	no dispersal	No
17	2080	SSP245	unlimited dispersal	Yes
18	2080	SSP245	unlimited dispersal	No
19	2080	SSP245	realistic dispersal	Yes
20	2080	SSP245	realistic dispersal	No
21	2080	SSP585	no dispersal	Yes
22	2080	SSP585	no dispersal	No
23	2080	SSP585	unlimited dispersal	Yes
24	2080	SSP585	unlimited dispersal	No
25	2080	SSP585	realistic dispersal	Yes
26	2080	SSP585	realistic dispersal	No